Relativistic multireference many-body perturbation theory calculations on Au^{64+} - Au^{69+} ions

M.J. Vilkas[1], Y. Ishikawa[1], and E. Träbert[2,3,a]

[1] Department of Chemistry, University of Puerto Rico, P.O. Box 23346, San Juan, Puerto Rico 00931-3346, USA
[2] Fakultät für Physik und Astronomie, Ruhr-Universität Bochum, 44780 Bochum, Germany
[3] Physics and Advanced Technologies, Lawrence Livermore National Laboratory, Livermore, CA 94550-9234, USA

Abstract. Many-body perturbation theory (MBPT) calculations are an adequate tool for the description of the structure of highly charged multi-electron ions and for the analysis of their spectra. We demonstrate this by way of a re-investigation of $n = 3$, $\Delta n = 0$ transitions in the EUV spectra of Na-, Mg-, Al-like, and Si-like ions of Au that have been obtained previously by heavy-ion accelerator based beam-foil spectroscopy. We discuss the evidence and propose several revisions on the basis of our multi-reference many-body perturbation theory calculations of Ne- through P-like ions of Au.

PACS. 32.30.Jc Visible and ultraviolet spectra – 31.15.Md Perturbation theory – 34.50.Fa Electronic excitation and ionization of atoms (including beam-foil excitation and ionization)

1 Introduction

Until very recently, a rule of thumb held that only one- and two-electron ions could be calculated well up to the highest values of the nuclear charge Z. Recent precise measurements on Li- and Be-like ions [1,2], Na-like ions [3], and Cu-like ions [4,5] up to $Z = 92$ confirm that there are accurate calculations of these few-electron ions and of ions with a single valence shell electron, too [6–8]. Ions with more than one valence shell electron used to fare much more poorly in such calculations [5,9,10], but there is notable recent progress [11].

On the experimental side, tokamaks (low-density plasma), laser-produced plasmas (high-density), and foil-excited ion beams (excitation at high density, observation in a low-density environment) have successively reached ever higher charge state ions, and the most recent addition to the spectroscopy tool box, the electron beam ion trap, can produce any charge state ion of any element. In most spectroscopic observations with the aforementioned devices, the spectra are much richer than asked for, and suitable theoretical support in the quest for spectral line identification would be useful. However, the validity of such calculations needs to be established by comparison to validated atomic structure data. These exist for many ions of elements up to $Z = 28$, and for much fewer ions and a few levels for ions up to about Xe ($Z = 54$), but they are very rare beyond.

The aim of our present report is a juxtaposition and discussion of available experimental data and new calculational results for a range of highly charged Au ($Z = 79$) ions. We expand on the interplay of experimental systematics and theoretical treatment of isoelectronic sequences far beyond the range of nuclear charge Z for which experimental data analysis has established firm ground and previous calculations have been tested. As experimental data we mainly use spectra that have been recorded in beam-foil spectroscopic experiments on Xe and Au about a decade ago [12–14]. (E.T., the lead author of those three studies, is a coauthor on the present report, and laboratory notes and other unpublished material of the time are available to us for a re-investigation.) We have discussed a similar situation for Xe elsewhere [15]. The extension of experimental spectrum analysis and calculations to Au, however, is a significant step that merits separate treatment, as will be shown presently.

2 Overview

In the spectra of highly charged ions, relativity plays a dominant role [16], and QED contributions are notable. In this they differ from the ions of lower charge, and it is not guaranteed that a given atomic structure calculation which may be in good agreement with experimental findings in one range will be equally reliable in the other. The same problem affects the interpretation of experimental data. It may be straightforward to exploit similarities in the spectra of neighbouring ions within the validated data

[a] e-mail: traebert@ep3.rub.de

range in an isoelectronic sequence. However, when trying to bridge wide gaps in an isoelectronic sequence, or when trying for substantial extrapolation, such pattern recognition based on comparison with either experimental data or with the results of computations (if available at all) may fail. The underlying problems may lie with either the experiment, with the calculations, or with both. We show examples below.

The production of highly charged ions of heavy elements has to provide the energy to exceed the ionization potentials of all lower charge states. This can be achieved by heat (thermal motion of particles, usually electrons) in low-density (tokamak) or high-density (laser-produced) plasmas, or by unidirectionally moving particles, either fast ions through a stationary electron gas (ion beam – foil interaction) or fast electrons through a stationary ion cloud (electron beam ion trap). The heaviest element for which Na-like ions (as a typical example of the ions that we wish to discuss) have been produced in a low-density plasma (tokamak) appears to be Nd ($Z = 60$) [17] (X-ray lines of Ne-like ions have been reported from this work, so Na-like ions must have been produced as well); Seely and Wagner discuss tokamak data up to Xe ($Z = 54$), Beiersdorfer et al. give wavelength data for La ($Z = 57$); the heaviest Na-like ion reported from a laser-produced plasma may be Gd ($Z = 64$) [20,21]. Both, foil-excited ion beams [22] and electron beam ion traps [23], have produced bare U ($Z = 92$) nuclei. Hence both techniques can provide Na-like ions of any lighter element more easily than that. In fact, accurate electron beam ion trap data for the $3s_{1/2}$-$3p_{3/2}$ transition in the Na-like ion Pt^{67+} ($Z = 78$) [24] have yielded a value of 5.32 ± 0.05 eV for the radiative (QED) contributions. Two subsequent measurements, one with a fast-ion beam and one using an electron beam ion trap, have focused on the $3s_{1/2}$-$3p_{3/2}$ transition in the Na-like ion Pb^{71+} ($Z = 82$) [25,26]. However, these measurements did not quite reach accuracy of the platinum measurement. The electron beam ion trap has since reached up to Na-like U^{81+}, where the QED contributions are larger than for Pt and Pb, improving the precision of the experimental determination of the radiative corrections to 0.2% [3].

The $3s_{1/2}$-$3p_{3/2}$ transitions in such heavy ions lie in the X-ray range; here we are concerned with the extreme ultraviolet (EUV) spectral range into which the $3s_{1/2}$-$3p_{1/2}$ transitions in various ions fall. Various experimenters have compared their findings with the results of calculations, and they have performed their own calculations in order to systematize the new data and to find a smooth trend underlying the data. For example, when Seely et al. [21] used the Grant code [27,28] in its default mode for their MCDF calculations, they tried to improve the agreement at high Z with their own laser-produced plasma data by estimating a semiempirical correction to their calculation. Measurements by other techniques later on agreed with the predictions of elaborate *ab initio* (that is, uncorrected) calculations ([7,8], see [3]). This finding suggested that the semiempirical correction introduced by Seely et al. reflected a systematic error in their laser-
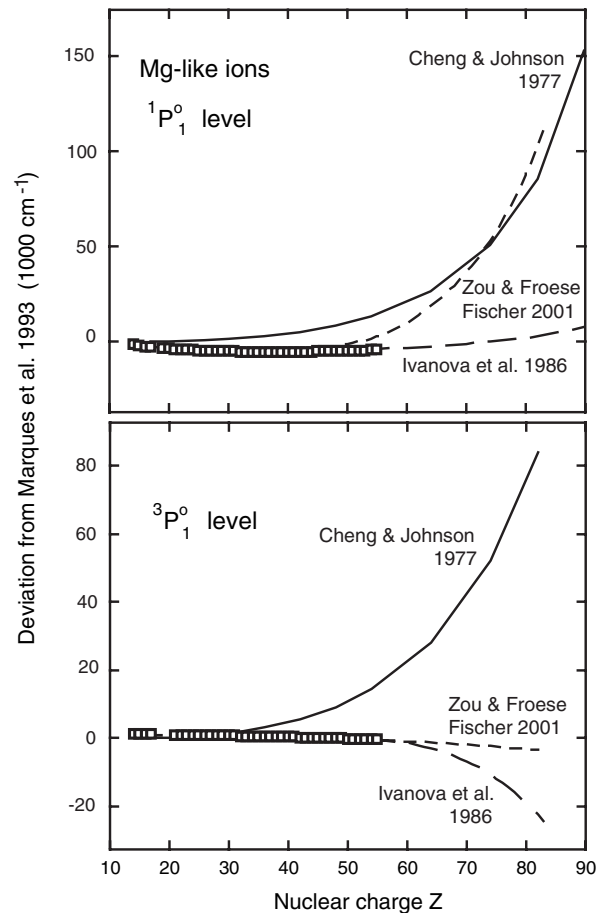

Fig. 1. Deviation of measured (open squares) and three calculated [29,30,32] level positions (ground state transition energies) of the (a) $3s3p$ $^1P_1^o$ and (b) $3s3p$ $^3P_1^o$ level in Mg-like ions from a fourth prediction [31].

produced plasma measurements, not a shortcoming of the calculations. Similar observations pertain to the Cu isoelectronic sequence [4,5].

While the systematics of the fundamental transitions in the Na isoelectronic sequence seem settled, the situation in the Mg sequence has been somewhat confusing. The $3s^2$ $^1S_0$ - $3s3p$ $^1P_1^o$ resonance transition in any Mg-like ion ought to lie close in wavelength to the $3s_{1/2}$-$3p_{3/2}$ transition in the Na-like ion of the same element, and the $3s^2$ $^1S_0$ - $3s3p$ $^3P_1^o$ intercombination transition ought to lie close in wavelength to the $3s_{1/2}$-$3p_{1/2}$ transition in the Na-like ion of the same element. However, not all experiments on Na-like ions report the nearby lines of Mg-like ions. For theory, there is the problem of a second electron in the valence shell. There exist a fair number of calculations of Mg-like ions in the low-Z range where there also are plenty of experimental data. Finding agreement with experiment in the low-Z range, however, is no guarantee for similar success in the high-Z range. In Figure 1 we intercompare several calculations for Mg-like ions [29–32] that reach to high values of Z (there exist even more calculations, and, in addition, there are semiempirical extrapolations like [33]). The calculated level energies roughly agree with

each other (and with experiment) at low Z, but the calculational trends diverge notably beyond Xe. This happens, although there is no doubt that at high Z only relativistic codes are appropriate and although MCDF calculations typically converge faster at high Z. Moreover, there is no simple finding like "new calculations do better than old ones" – some old ones turn out to be good, and some new ones not so good.

Among the few observations of spectra of highly charged high-Z ions with an $n = 3$ valence shell are the Xe ($Z = 54$) and Au ($Z = 79$) data that were obtained by beam-foil spectroscopy at the GSI Darmstadt Unilac accelerator some ten years ago [12–14]. The experiments pushed the envelope of such investigations at the time; the primary interest was in the transition rates of the $3s - 3p - 3d$ transitions of the Na-like ions, but radiative decay curves of other transitions in the spectral field-of-view of the detection system were recorded and analyzed as well. The data on Xe [12,13] have been re-investigated elsewhere [15]. Concerning the isoelectronic sequences of ions with more than a single electron in the valence shell, there were only very few predictions available at the time that reached as high in Z as Au. Of the predictions for Mg-like ions, one predicted a line on the short-wavelength side of the corresponding Na-like ion, and another calculation predicted the same transition on the long-wavelength side. Better calculations and other insights suggest that the experimenters at the time made a wrong choice on which calculation to trust for the assignment of these key lines. We have applied our calculational techniques to Au in order to provide a consistent body of atomic structure information on Ne- through P-like ions of Au and to re-investigate these beam-foil data on Au [13,14].

3 Theory

In our calculations, we have developed a Multi-Reference Møller-Plesset (MR-MP) scheme, a variant of Many-Body Perturbation Theory (MBPT). The effective N-electron Hamiltonian (in atomic units) for the development of our relativistic MR-MP algorithm is taken to be the relativistic "no-pair" Dirac-Coulomb-Breit (DCB) Hamiltonian [34,35]

$$H_{DCB}^+ = \sum_i h_D(i) + \mathcal{L}_+ \left(\sum_{i>j} \frac{1}{r_{ij}} + B_{ij}(0) \right) \mathcal{L}_+ \quad (1)$$

with

$$B_{ij}(0) = -\frac{1}{2}[\boldsymbol{\alpha}_i \cdot \boldsymbol{\alpha}_j + (\boldsymbol{\alpha}_i \cdot \mathbf{r}_{ij})(\boldsymbol{\alpha}_j \cdot \mathbf{r}_{ij})/r_{ij}^2]/r_{ij}. \quad (2)$$

Here $h_D(i)$ is the Dirac one-electron Hamiltonian. The DCB Hamiltonian is covariant to first order and increases the accuracy of calculated fine-structure splittings and inner-shell binding energies. Higher order QED effects appear first in order α^3. The nucleus is modeled as a sphere of uniform proton charge distribution. $\mathcal{L}_+ =$ $L_+(1)L_+(2)\dots L_+(N)$, where $L_+(i)$ is the projection operator onto the space $D^{(+)}$ spanned by the positive-energy eigenfunctions of the matrix Dirac-Fock-Breit (DFB) SCF equation [35]. $\mathcal{L}_+$ is the projection operator onto the positive-energy space $\mathfrak{D}^{(+)}$ spanned by the N-electron configuration-state functions (CSF) constructed from the positive-energy eigenfunctions of the matrix DFB SCF. It takes into account the field-theoretic condition that the negative-energy states are filled. The eigenfunctions $\{\phi_{n_q\kappa_q}^{(\pm)}(r)\}(\in D^{(+)} \cup D^{(-)})$ of the matrix DFB SCF equation clearly separate into two discrete manifolds, $D^{(+)}$ and $D^{(-)}$, respectively, of positive- and negative-energy one-particle states. As a result, the positive-energy projection operators can be accommodated easily in many-body calculations. The formal conditions on the projection are automatically satisfied when only the positive-energy spinors are employed.

N-electron eigenfunctions of the no-pair DCB Hamiltonian are approximated by a linear combination of M_{MC} configuration-state functions, $\{\Phi_I^{(+)}(\gamma_I \mathcal{J}\pi); I = 1, 2, \dots, M_{MC}\} \in \mathfrak{P}^{(+)}$, constructed from positive-energy eigenfunctions of the matrix multiconfiguration Dirac-Fock-Breit (MCDFB) SCF equation,

$$\psi_\kappa^{MC}(\gamma_K \mathcal{J}\pi) = \sum_I^{M_{MC}} C_{IK}\Phi_I^{(+)}(\gamma_I \mathcal{J}\pi). \quad (3)$$

The MCDFB SCF wave function $\psi_\kappa^{MC}(\gamma_K \mathcal{J}\pi)$ is an eigenfunction of the angular momentum and parity operators with total angular momentum $\mathcal{J}$ and parity π. γ denotes a set of quantum numbers other than $\mathcal{J}$ and π necessary to specify the state uniquely. In our present calculations, the set of configuration state functions (Eq. (3)) are generated by "$n = 3$ CAS" — a complete set of configuration-state functions generated within the $n = 3$ subspace.

Second-order variation of the state-averaged energy $\Omega_{state-ave}$ [36] is taken with respect to the matrix elements of spinor unitary rotation matrix and configuration mixing coefficients $\{C_{IK}\}$, leading to the Newton-Raphson equations for second-order MCDFB SCF [37]. This state-averaged second-order MCDFB equations yields a single set of spinors for the ground and low-lying even- and odd-parity excited $(\gamma, \mathcal{J}, \pi)$ levels.

In order to account for strong configuration mixing among the highly excited levels, the multireference configuration interaction method (MR-CI) [38] is introduced in an extended subspace $\mathfrak{P}_{CI}^{(+)}$ of positive-energy space. N-electron eigenfunctions of the no-pair DCB Hamiltonian are approximated by a linear combination of M_{CI} ($\gg M_{MC}$) configuration-state functions, $\{\Phi_I^{(+)}(\gamma_I \mathcal{J}\pi); I = 1, 2, \dots, M_{CI}\}$, constructed from the one-particle positive-energy spinors computed in matrix MCDFB SCF. Variation of the configuration-state coefficients $\{C_{IK}\}$ leads to the determinantal CI equation

$$\det \left(\langle \Phi_I^{(+)}(\gamma_I \mathcal{J}\pi) \mid H_{DCB}^+ \mid \Phi_J^{(+)}(\gamma_J \mathcal{J}\pi) \rangle \right.$$
$$\left. - E^{CI}\langle \Phi_I^{(+)}(\gamma_I \mathcal{J}\pi) \mid \Phi_J^{(+)}(\gamma_J \mathcal{J}\pi) \rangle \right) = 0. \quad (4)$$

The eigenfunctions $\{\psi_K^{CI}(\gamma_K \mathcal{J}\pi)\}$ form a subspace $\mathfrak{P}_{CI}^{(+)}$ of the positive-energy space $\mathfrak{D}^{(+)}$

$$\psi_K^{CI}(\gamma_K \mathcal{J}\pi) = \sum_I^{M_{CI}} C_{IK} \Phi_I^{(+)}(\gamma_I \mathcal{J}\pi), \ K = 1, 2, ... M_{CI}. \tag{5}$$

The total DCB energy of the general CI state $|\psi_K^{CI}(\gamma_K \mathcal{J}\pi)\rangle$ can be expressed as

$$E_K^{CI}(\gamma_K \mathcal{J}\pi) = \langle \psi_K^{CI}(\gamma_K \mathcal{J}\pi) | H_{DCB}^+ | \psi_K^{CI}(\gamma_K \mathcal{J}\pi) \rangle$$

$$= \sum_{I,J=1}^{\mathfrak{P}_{CI}(+)} C_{IK} C_{JK} \langle \Phi_I^{(+)}(\gamma_I \mathcal{J}\pi) | H_{DCB}^+ | \Phi_J^{(+)}(\gamma_J \mathcal{J}\pi) \rangle. \tag{6}$$

Here it is assumed that $\psi_K^{CI}(\gamma_K \mathcal{J}\pi)$ and $\Phi_I^{(+)}(\gamma_I \mathcal{J}\pi)$ are normalized.

The frequency-dependent Breit interaction, normal mass shift (NMS) and specific mass shift (SMS) are evaluated as the first-order corrections using the eigenvectors $\{\psi_K^{CI}(\gamma_K \mathcal{J}\pi)\}$ from the MR-CI [36]. The frequency dependence of the Breit interaction is evaluated in the Coulomb gauge, subtracting frequency-independent Breit interaction which is already included ($B^{(0+1)}(0)$) in MR-CI (Eq. (6)). The first-order corrections calculated in this way are denoted $\Delta B^{(1)}(\omega)$.

The no-pair DCB Hamiltonian H_{DCB}^+ is decomposed into two parts, unperturbed Hamiltonian H_0 and perturbation V, following Møller and Plesset [39],

$$H_{DCB}^+ = H_0 + V, \tag{7}$$

$$H_0 = \sum_I^{\mathfrak{D}(+)} |\Phi_I^{(+)}(\gamma_I \mathcal{J}\pi)\rangle E_I^{CSF} \langle \Phi_I^{(+)}(\gamma_I \mathcal{J}\pi)|, \tag{8}$$

so that

$$H_0 |\Phi_I^{(+)}(\gamma_I \mathcal{J}\pi)\rangle = E_I^{CSF} |\Phi_I^{(+)}(\gamma_I \mathcal{J}\pi)\rangle \quad (I = 1, 2, \ldots). \tag{9}$$

E_I^{CSF} is a sum of the products of one-electron energies defined by ε_q^+ and an occupation number $n_{n_q \kappa_q}[I]$ of the κ_q-symmetry shell in the CSF $\Phi_I^{(+)}(\gamma_I \mathcal{J}\pi)$ [40,41];

$$E_I^{CSF} = \sum_q^{D(+)} \varepsilon_q^+ n_{n_q \kappa_q}[I]. \tag{10}$$

The subset, $\{\Phi_I^{(+)}(\gamma_I \mathcal{J}\pi); I = 1, 2, \ldots, M_{CI}\}$, with which we expand the CI wavefunction $\psi_K^{CI}(\gamma_K \mathcal{J}\pi)$ (Eq. (5)) defines an active subspace $\mathfrak{P}_{CI}^{(+)}$ spanned by $\psi_K^{CI}(\gamma_K \mathcal{J}\pi)$ and its $M_{CI} - 1$ orthogonal complements, $\{\psi_K(\gamma_K \mathcal{J}\pi); K = 1, 2, \ldots, M_{CI}\}$. The matrix of H_{DCB}^+ in this subspace is diagonal

$$\langle \psi_K^{CI}(\gamma_K \mathcal{J}\pi) | H_{DCB}^+ | \psi_L^{CI}(\gamma_L \mathcal{J}\pi) \rangle = \delta_{KL} \left(E_K^{(0)} + E_K^{(1)} \right)$$

$$= \delta_{KL} E_K^{CI}(\gamma_K \mathcal{J}\pi), \tag{11}$$

where

$$E_K^{(0)} = \langle \psi_K^{CI}(\gamma_K \mathcal{J}\pi) | H_0 | \psi_K^{CI}(\gamma_K \mathcal{J}\pi) \rangle$$

$$= \sum_I^M C_{IK} C_{IK} E_I^{CSF} \tag{12}$$

and

$$E_K^{(1)} = \langle \psi_K^{CI}(\gamma_K \mathcal{J}\pi) | V | \psi_K^{CI}(\gamma_K \mathcal{J}\pi) \rangle. \tag{13}$$

The residual space in the positive-energy subspace is $\mathfrak{Q}^{(+)} = \mathfrak{D}^{(+)} - \mathfrak{P}_{CI}^{(+)}$, which is spanned by CSFs $\{\Phi_I^{(+)}(\gamma_I \mathcal{J}\pi); I = M_{CI} + 1, M_{CI} + 2, \ldots\}$.

Application of Rayleigh-Schrödinger perturbation theory provides order-by-order expressions of the perturbation series for the state approximated by $|\psi_K^{CI}(\gamma_K \mathcal{J}\pi)\rangle$,

$$E_K(\gamma_K \mathcal{J}\pi) = E_K^{CI}(\gamma_K \mathcal{J}\pi) + E_K^{(2)} + \ldots, \tag{14}$$

where

$$E_K^{(2)} = \langle \psi_K^{CI}(\gamma_K \mathcal{J}\pi) | V \mathcal{R} V | \psi_K^{CI}(\gamma_K \mathcal{J}\pi) \rangle. \tag{15}$$

Here, $\mathcal{R}$ is the resolvent operator,

$$\mathcal{R} = \frac{\mathcal{Q}^{(+)}}{E_K^{CSF} - H_0} \tag{16}$$

with

$$\mathcal{Q}^{(+)} = \sum_I^{\mathfrak{Q}(+)} |\Phi_I^{(+)}(\gamma_I \mathcal{J}\pi)\rangle \langle \Phi_I^{(+)}(\gamma_I \mathcal{J}\pi)|. \tag{17}$$

The projection operator $\mathcal{Q}^{(+)}$ projects onto the subspace $\mathfrak{Q}^{(+)}$ spanned by CSFs $\{\Phi_I^{(+)}(\gamma_I \mathcal{J}\pi); I = M_{CI} + 1, M_{CI} + 2, \ldots\}$. Using the spectral resolution of the resolvent operator acting on $V|\Phi_I^{(+)}(\gamma_I \mathcal{J}\pi)\rangle$, the second-order correction may be expressed as,

$$E_K^{(2)} = \sum_{IJ} C_{IK} C_{JK} \langle \Phi_I^{(+)}(\gamma_I \mathcal{J}\pi) | V \mathcal{R} V | \Phi_J^{(+)}(\gamma_J \mathcal{J}\pi) \rangle$$

$$= \sum_{L=M+1}^{\mathfrak{Q}(+)} \sum_{I,J=1}^{\mathfrak{P}_{CI}(+)} C_{IK} C_{JK} \frac{\langle \Phi_I^{(+)}(\gamma_I \mathcal{J}\pi) | V | \Phi_L^{(+)}(\gamma_L \mathcal{J}\pi) \rangle}{E_J^{CSF} - E_L^{CSF}}$$

$$\times \langle \Phi_L^{(+)}(\gamma_L \mathcal{J}\pi) | V | \Phi_J^{(+)}(\gamma_J \mathcal{J}\pi) \rangle. \tag{18}$$

In this form, all perturbation corrections beyond first order describe residual dynamic correlation correction for the state approximated by the CI wavefunction $|\psi_K^{CI}(\gamma_K \mathcal{J}\pi)\rangle$.

Summations over the CSFs in equations (16) and (18) are restricted to CSFs ($\in \mathfrak{D}^{(+)}$) constructed from the positive-energy branch ($D^{(+)}$) of the spinors, effectively incorporating into the computational scheme the "no-pair" projection operator $\mathcal{L}_+$ contained in the DCB Hamiltonians.

The large and small radial components of the Dirac spinors are expanded in sets of even-tempered Gaussian-type functions (GTF) that satisfy the boundary conditions associated with the finite nucleus [42]. The speed of

light is taken to be 137.0359895 a.u. throughout this study. The GTFs that satisfy the boundary conditions associated with the finite nucleus are automatically kinetically balanced [42]. Even-tempered basis sets of $26s24p20d18f$ G spinors (G for "Gaussian") for up to angular momentum $L = 3$ and 15 G spinors for $L = 4$–11 are employed. The order of the partial-wave expansion L_{max}, the highest angular momentum of the spinors included in the virtual space, is $L_{max} = 11$ throughout this study. The nuclei were simulated as spheres of uniform proton charge with the radii $R = 2.2677 \times 10^{-5} A^{1/3}$, where A is the atomic mass in amu and R is measured in Bohr.

All electrons have been included in the MR-MP perturbation theory calculations to determine accurately the effects of relativity on electron correlation. Radiative corrections, the Lamb shifts, were estimated for each state by evaluating the electron self-energy and vacuum polarization following an approximation scheme discussed by Indelicato, Gorceix, and Desclaux [43]. The code described in references [43,44] was adapted to our basis set expansion calculations for this purpose: all the necessary radial integrals were evaluated analytically. In this scheme [44], the screening of the self energy is estimated by integrating the charge density of a spinor to a short distance from the origin, typically 0.3 Compton wavelength. The ratio of the integral computed with an MCDFB SCF spinor and that obtained from the corresponding hydrogenic spinor is used to scale the self-energy correction for a bare nuclear charge that has been computed by Mohr [45]. The second-order correlation corrections $E(2)$ are on the order of $1000\,\mathrm{cm}^{-1}$ for all levels but one in Si-like Au. For highly ionized ions, such as Au^{64+} – Au^{69+}, the perturbation series converges very rapidly and the higher order correlation corrections are negligible, much less than $100\,\mathrm{cm}^{-1}$.

The MCDFB SCF employs a complete active space (CAS) within the $n = 3$ subspace. While we employ extensive MBPT wave functions in the calculation of term energies, the transition rates have mostly be calculated in the less time-consuming, but often also less accurate Multi-Configuration Dirac-Fock (MCDF) formalism. Often the two approaches yield transition rates that agree with each other to better than 1% (and the results of calculations in Babushkin (length) and Coulomb (velocity) gauges often are similarly close to each other). However, especially in cases with small transition probabilities (long level lifetimes), the differences can be larger (up to 10% in our calculations)). We quote our transition rates and lifetime results to three significant figures, but we consider the present results as no more than useful approximations that, if needed, should be improved upon by more extensive MBPT calculations.

4 Notes on the results of our and other calculations

4.1 Ne-like ions

The ground state of Ne-like gold is a closed shell $1s^2 2s^2 2p^6$ $^1S_0$ system. The lowest excited states have excitations

from the $n = 2$ core to the $n = 3$ valence electrons. Previous experimental studies were mostly concentrated on the X-ray transitions of the $2p_{1/2}^{-1}3s$ to the ground $1s^2 2s^2 2p^6$ $^1S_0$ state. The lowest excited state is located at about 10 keV. The dominant decays hence appear in the X-ray region with wavelengths of 0.8–1.4 Å. There are numerous theoretical calculations of Ne-like ions. Cogordan and Lunell [46] performed Dirac-Fock calculations for the neonlike ions up to Xe^{44+}. Hagelstein and Jung [47] performed relativistic distorted-wave calculations of the electron collision cross sections for Fe, Se, Y, Mo, and Ag. Zhang and Sampson [48] extended their work to include ions with $22 \leq Z \leq 92$, using the Dirac-Fock-Slater approximation; the accuracy of the calculated transition energies is expected to be poorer than that of the Dirac-Fock formalism used in [47]. In 1989, Aglitskii et al. [49] presented both theoretical and experimental results. The theoretical approximations were based on a model potential and used hydrogenic perturbation theory (PT), implemented in the form of the MZ code [50,51]. Experimental data were summarized for ions up to Bi^{73+}. For high-Z ions $Z \geq 60$ both theoretical approximations failed to describe accurately the $\Delta n = 0$ transition energies. Perturbational corrections have been added later by Ivanova and Gulov [52]. They also calculated all allowed and forbidden transition rates to the ground state. Quinet, Gorlia and Biémont [53] performed multiconfigurational Dirac-Fock calculations, corrected by a semi-empirical procedure for neonlike ions up to U^{82+}. There were only few experimental studies for very high-Z ions at that time, and semiempirical adjustments were not reliable in this range of very high nuclear charges. Safronova, Safronova and Bruch [54] estimated higher-order corrections in their hydrogenic PT expansion, and they concluded that an agreement of 3 to 4 digits in the energy values signifies the limit of accuracy of the calculations by the MZ, MP, and MCHFP methods. For the relatively small term differences associated with $\Delta n = 0$ transitions, those theoretical approximations are not reliable. In 2001, Safronova et al. [55] applied the MBPT method (using a Dirac-Fock potential) to calculate energy levels and radiative decay rates of selected neonlike ions up to $Z = 100$, in the most accurate theoretical calculation on such ions up to now.

Experimental data on very-high Z Ne-like ions were published based on observations at the Princeton Large Torus (PLT) tokamak [17], foil-excited ion beams [56,57], and an electron beam ion trap (EBIT) [58]. In this paper we will make use of the Au^{69+} measurements by Chandler et al. [56]. (The beam-foil observations by Träbert et al. [13,14] do not comprise lines associated with Ne-like ions of Au.) In the Chandler et al. paper on X-ray spectroscopic observations of neonlike gold [56], several X-ray decays to the ground state have been identified guided by MCDF calculations. In Table 1 we include MCDF and MBPT calculated values. While the resolution in this experiment (beam-foil) was quite poor, the second-order perturbation theory calculations (MBPT and MR-MP) agree better than the MCDF results with the experimental transition energies of the levels with the $2p_{1/2}^{-1}$

Table 1. Comparison of the MR-MP calculated excitation energies E (eV) and lifetimes τ with experimental and other theoretical results in Ne-like gold ions. The experimental results are given with error estimates. Lifetimes were evaluated by first-order wavefunctions.

State	E (MR-MP)	τ (ps)	E (Expt)[a]	E (MCDF)[a]	E (MBPT)[b]
$1s^2 2s^2 2p^6\{0\}$	0			0	0	0
$2p_{3/2}^{-1}3s_{1/2}\{2\}$	9497.2	149			9495.7
$2p_{3/2}^{-1}3s_{1/2}\{1\}$	9506.4	0.0051	9506.5(4.5)	9505.3	9505.2
$2p_{3/2}^{-1}3p_{1/2}\{1\}$	9662.5	24.1			
$2p_{3/2}^{-1}3p_{1/2}\{2\}$	9663.9	24.8	9666.7(4.5)	9663.6	9662.8
$2p_{3/2}^{-1}3p_{3/2}\{3\}$	10179.6	0.0246			
$2p_{3/2}^{-1}3p_{3/2}\{1\}$	10180.2	0.336			
$2p_{3/2}^{-1}3p_{3/2}\{2\}$	10193.9	0.306	10190.0(4.9)	10193.6	10192.6
$2p_{3/2}^{-1}3p_{3/2}\{0\}$	10255.2	0.234			
$2p_{3/2}^{-1}3d_{3/2}\{0\}$	10353.0	0.449			
$2p_{3/2}^{-1}3d_{3/2}\{3\}$	10363.6	0.431			
$2p_{3/2}^{-1}3d_{3/2}\{1\}$	10363.7	0.0064	10357.9(5.2)	10363.7	10361.3
$2p_{3/2}^{-1}3d_{3/2}\{2\}$	10372.9	0.415			
$2p_{3/2}^{-1}3d_{5/2}\{4\}$	10477.7	4.43			
$2p_{3/2}^{-1}3d_{5/2}\{2\}$	10485.6	4.25			
$2p_{3/2}^{-1}3d_{5/2}\{3\}$	10496.4	4.08			
$2p_{3/2}^{-1}3d_{5/2}\{1\}$	10527.0	0.0005	10519.7(5.4)	10527.7	10526.5
$2p_{1/2}^{-1}3s_{1/2}\{0\}$	11376.1	60.1			
$2p_{1/2}^{-1}3s_{1/2}\{1\}$	11379.5	0.0237	11374.8(6.2)	11377.5	11378.4
$2p_{1/2}^{-1}3p_{1/2}\{1\}$	11536.3	19.2			
$2p_{1/2}^{-1}3p_{1/2}\{0\}$	11589.1	2.27			
$2s_{1/2}^{-1}3s_{1/2}\{1\}$	11907.9	0.0245			
$2s_{1/2}^{-1}3s_{1/2}\{0\}$	11948.3	0.0253			
$2p_{1/2}^{-1}3p_{3/2}\{2\}$	12063.2	0.320			12062.3
$2p_{1/2}^{-1}3p_{3/2}\{1\}$	12065.8	0.212			
$2s_{1/2}^{-1}3p_{1/2}\{1\}$	12078.0	0.0014	12071.6(6.9)	12081.4	12076.1
$2s_{1/2}^{-1}3p_{1/2}\{0\}$	12079.0	0.0240			
$2p_{1/2}^{-1}3d_{3/2}\{2\}$	12242.6	0.423			
$2p_{1/2}^{-1}3d_{3/2}\{1\}$	12268.4	0.0005	12260.8(7.1)	12268.5	12266.9
$2p_{1/2}^{-1}3d_{5/2}\{2\}$	12364.0	2.69			
$2p_{1/2}^{-1}3d_{5/2}\{3\}$	12367.4	4.14			
$2s_{1/2}^{-1}3p_{3/2}\{2\}$	12598.7	0.0223			
$2s_{1/2}^{-1}3p_{3/2}\{1\}$	12605.3	0.0021	12600.2(7.5)	12608.6	12603.0
$2s_{1/2}^{-1}3d_{3/2}\{1\}$	12777.6	0.0248			
$2s_{1/2}^{-1}3d_{3/2}\{2\}$	12783.0	0.0233			
$2s_{3/2}^{-1}3d_{5/2}\{3\}$	12895.3	0.0247			
$2s_{1/2}^{-1}3d_{5/2}\{2\}$	12911.6	0.0257	12909.6(7.8)	12915.8	12909.1

[a] Reference [56]. [b] Reference [55].

and $2s_{1/2}^{-1}$ cores. The MCDF results are nearly identical to those of our correlated calculations for $2p_{3/2}^{-1}$.

4.2 Na-like ions

Na-like ions have only few levels arising from configurations with the single valence electron (Tab. 2). The E1 decays of those energy levels result in few, well separated spectral lines. Theoretically, systems with a single valence electron have been investigated by various highly correlated methods. In 1988, Johnson, Blundell and Sapirstein [59] applied MBPT to calculate energy levels along the sodium isolelectronic sequence. They included third-order Coulomb and Breit interaction corrections. For low-Z ions, the results perfectly agreed with experimental data, and only few theoretical studies have been done to improve on the existing MBPT calculation. For high-Z ions, the systematic deviation was attributed to QED corrections. Kim, Baik, Indelicato and Desclaux [7] have done a systematic study of Na-like ions and have presented interpolated and extrapolated transition energies. Similar

Table 2. Comparison of the MR-MP calculated excitation energies E (cm^{-1}) and lifetimes τ with other theoretical results in Na-like gold ions. Lifetimes were evaluated by first-order wavefunctions.

State	E (cm^{-1})	τ (ps)	E (MCDF)^a
3s{1/2}	0		0
$3p_{1/2}${1/2}	1428506	0.459	1429101
$3p_{3/2}${3/2}	5542749	20.2	5543326
$3d_{3/2}${3/2}	7179829	0.399	
$3d_{5/2}${5/2}	8106367	3.65	

^{a} Reference [7].

(but systematically deviant) predictions were made by Seely and Wagner [18] based on the Grant (MCDF) code. Finally, Blundell in 1993 presented ab initio estimates of screened self-energy and vacuum polarization for ns-np transitions in Li-like, Na-like and Cu-like ions [8]. The Blundell calculations agree well with phenomenological estimates of the QED terms by Kim et al. [7]; the results of both calculations match accurate observations up to $Z = 92$ [3].

In the beam-foil experiment [13], the Na-like Au ion line ($3p$ ^{2}P$^o_{1/2}$ level decay) with a calculated wavelength of 69.97 Å [7] was used as an in-beam reference line. However, as is explained below, the wrong observed line was identified with this transition. The recalibrated spectra are shown and explained below.

4.3 Mg-like ions

Mg-like ions have only two valence electrons and are relatively simple atomic system to treat theoretically. In the overview section and Figure 1 we have shown how different in spite of the relative simplicity the high-Z trends of four calculations [29–32] are. Experimental data on Mg-like ions in laser-produced plasmas reach up no farther than to Cs ($Z = 55$) [60–62]. The most accurate calculations on the Mg-like ions apparently have been done by Safronova, Johnson and Berry in 2000 [63,64], using a standard MBPT procedure, including second-order Coulomb correction and Lamb shift. (It is not clear whether first-order frequency-dependent and second-order Breit corrections were taken into account.) The numerical values in that paper were presented only for ions with $Z \le 42$. However, the authors made a remark about the Mg-like Au ($Z = 79$) line identified by Träbert et al. [13] at 67.1 Å. Both highly-correlated theoretical methods predict this line at 71.866 Å (MR-MP) and 71.806 Å (MBPT). In addition to the large disagreement in line wavelength, the measured lifetime is much shorter than the theoretical values. These clues suggest that the line at 67.1 Å has been misidentified (as is confirmed and discussed in more detail below). In Table 3 the energy levels of the $n = 3$ complex are presented. There are two levels — $3s3p_{3/2}$ $J = 1$ (^{3}P$^o_1$ in LS-coupling) with a calculated lifetime of 43 ps, and $3p_{1/2}3d_{3/2}$ $J = 2$ with a predicted level lifetime

Table 3. MR-MP calculated term values E (cm^{-1}) and lifetimes τ in Mg-like gold ions. Lifetimes were evaluated by first-order wavefunctions. The notation of some lifetimes like $a(b)$ refers to $a \times 10^b$.

State	E (cm^{-1})	τ (ps)	τ (ps)
$3s^2${0}	0		
$3s3p_{1/2}${0}	1252693		2.82(3)^a
$3s3p_{3/2}${1}	1391982	43.1	44.7^a
$3p^2_{1/2}${0}	2980699	6.41	
$3s3p_{3/2}${2}	5318176	1710	
$3s3p_{3/2}${1}	5641487	0.213	0.215^a
$3p_{1/2}3p_{3/2}${2}	6900798	1.29	
$3p_{1/2}3p_{3/2}${1}	6921347	0.290	
$3s3d_{3/2}${1}	7192761	0.356	
$3s3d_{3/2}${2}	7316163	0.195	
$3s3d_{5/2}${3}	8102408	2.870	
$3s3d_{5/2}${2}	8249904	1.499	
$3p_{1/2}3d_{3/2}${2}	8540369	16.1	
$3p_{1/2}3d_{3/2}${1}	8845718	0.268	
$3p_{1/2}3d_{5/2}${2}	9616195	2.47	
$3p_{1/2}3d_{5/2}${3}	9645293	0.344	
$3p^2_{3/2}${2}	11046813	0.149	
$3p^2_{3/2}${0}	11216520	0.152	
$3p_{3/2}3d_{3/2}${2}	12723019	0.167	
$3p_{3/2}3d_{3/2}${3}	12810425	0.180	
$3p_{3/2}3d_{3/2}${0}	12810512	0.162	
$3p_{3/2}3d_{3/2}${1}	12814377	0.164	
$3p_{3/2}3d_{5/2}${4}	13531906	0.329	
$3p_{3/2}3d_{5/2}${2}	13633044	0.278	
$3p_{3/2}3d_{5/2}${3}	13791460	0.270	
$3p_{3/2}3d_{5/2}${1}	13902832	0.252	
$3d^2_{3/2}${2}	14508299	0.189	
$3d^2_{3/2}${0}	14743568	0.175	
$3d_{3/2}3d_{5/2}${3}	15380459	0.343	
$3d_{3/2}3d_{5/2}${2}	15485306	0.316	
$3d_{3/2}3d_{5/2}${4}	15505924	0.383	
$3d_{3/2}3d_{5/2}${1}	15534393	0.308	
$3d^2_{5/2}${4}	16329731	1.65	
$3d^2_{5/2}${2}	16422316	1.38	
$3d^2_{5/2}${0}	16669509	1.04	

^{a} Reference [31].

of 16 ps — that is, with lifetimes in a range that is technically accessible by straightforward beam-foil spectroscopy. There also is one extremely long-lived level ($3s3p$ ^{3}P$^o_0$ in LS-coupling notation) that cannot decay by single photon emission at all, except by hyperfine interaction. As, indeed, ^{197}Au has a non-zero nuclear spin, hyperfine interaction shortens this level lifetime to 2.8 ms [31]. The $3s3p$ ^{3}P$^o_2$ level has a calculated lifetime in the nanosecond range. Hyperfine interaction must also play a role for the decay of this level, but a similar hyperfine-induced decay

Table 4. Second-order MR-MP transition probabilites of the forbidden M1/M2 and E2/E3 decays of some low-lying long-lived levels in Ne- to Si-like Au ions. Lifetimes were evaluated by first-order wavefunctions. The notation of the transition probabilities like $a(b)$ refers to $a \times 10^b\,\mathrm{s}^{-1}$; * denotes odd parity levels.

Ion	Upper	Lower	λ (Å)	type	A (s^{-1})	τ ps
Ne	2(1)*	0(1)	1.306	M2	6.72(9)	149
Mg	2(1)*	0(1)	18.803	M2	7.37(5)	
		0(2)	42.781	M2	7.51(1)	
		0(1)*	24.597	E2	9.97(6)	
		1(1)*	25.470	M1	5.59(8)	
				E2	1.36(7)	1710
Al	3/2(1)*	1/2(1)	39.866	E1	7.52(8)	
		1/2(1)*	24.019	M1	5.54(8)	
				E2	2.17(7)	753
Si	1(1)	0(1)	25.850	M1	6.82(8)	1470
Si	2(1)	0(1)	25.326	E2	1.60(7)	
		1(1)	1247.9	M1	2.46(3)	
				E2	2.62(−2)	62600
Si	2(2)	2(1)*	40.065	E1	1.39(10)	
		1(1)*	44.240	E1	1.03(10)	
		0(1)	13.484	E2	2.49(8)	
		1(1)	28.187	M1	2.46(3)	
				E2	1.44(4)	
		1(2)	1538.0	M1	5.37(3)	
				E2	5.22(−3)	
		2(1)	28.838	M1	3.06(5)	
				E2	1.35(4)	40.9
Si	2(3)	1(1)*	44.240	E1	1.11(9)	
		1(2)*	59.165	E1	1.39(8)	
		1(1)	24.924	M1	5.40(8)	
				E2	1.29(7)	
		1(2)	188.86	M1	4.70(3)	
				E2	3.55(−1)	
		2(1)	25.432	M1	5.33(8)	
				E2	2.84(7)	
		2(2)	215.292	M1	4.81(2)	
				E2	1.21(−1)	
		0(1)	12.689	E2	8.89(2)	423
Si	0(2)	1(1)*	41.017	E1	1.17(9)	
		1(2)*	53.538	E1	5.06(7)	
		1(1)	23.867	M1	1.19(9)	
		1(2)	141.41	M1	4.11(0)	416

Table 5. MR-MP calculated term values E (cm^{-1}) and lifetimes τ in Al-like gold ions. Lifetimes were evaluated by first-order wavefunctions.

State	E (cm^{-1})	τ (ps)
$3s^2 3p_{1/2}\{1/2\}$	0	
$3s 3p_{1/2}^2\{1/2\}$	1504645	21.5
$3s^2 3p_{3/2}\{3/2\}$	4013023	753
$3s 3p_{1/2} 3p_{3/2}\{3/2\}$	5247290	41.5
$3s 3p_{1/2} 3p_{3/2}\{5/2\}$	5408298	58.7
$3s 3p_{1/2} 3p_{3/2}\{3/2\}$	5586504	0.931
$3s 3p_{1/2} 3p_{3/2}\{1/2\}$	5677863	0.202
$3s^2 3d_{3/2}\{3/2\}$	6068556	0.147
$3s^2 3d_{5/2}\{5/2\}$	6881849	2.52
$3s 3p_{1/2} 3d_{3/2}\{3/2\}$	7048662	5.00
$3p_{1/2}^2 3p_{3/2}\{3/2\}$	7154878	1.27
$3s 3p_{1/2} 3d_{3/2}\{5/2\}$	7253386	29.5
$3s 3p_{1/2} 3d_{3/2}\{1/2\}$	7487922	0.250
$3s 3p_{1/2} 3d_{3/2}\{3/2\}$	7556495	0.159
$3s 3p_{1/2} 3d_{5/2}\{5/2\}$	8148852	2.64
$3s 3p_{1/2} 3d_{5/2}\{7/2\}$	8278197	3.40
$3s 3p_{1/2} 3d_{5/2}\{5/2\}$	8366219	2.91
$3s 3p_{1/2} 3d_{5/2}\{3/2\}$	8404265	1.09
$3p_{1/2}^2 3d_{3/2}\{3/2\}$	8926194	5.44
$3s 3p_{3/2}^2\{5/2\}$	9360518	0.827
$3s 3p_{3/2}^2\{1/2\}$	9690030	0.280
$3s 3p_{3/2}^2\{3/2\}$	9751078	0.138
$3p_{1/2} 3d_{5/2}\{5/2\}$	9957562	2.41
$3p_{1/2} 3p_{3/2}^2\{5/2\}$	11004843	0.520
$3p_{1/2} 3p_{3/2}^2\{3/2\}$	11052846	0.192
$3p_{1/2} 3p_{3/2}^2\{1/2\}$	11205754	0.250
$3s 3p_{3/2} 3d_{3/2}\{3/2\}$	11267850	0.230
$3s 3p_{3/2} 3d_{3/2}\{1/2\}$	11282032	0.312
$3s 3p_{3/2} 3d_{3/2}\{5/2\}$	11314235	0.178
$3s 3p_{3/2} 3d_{3/2}\{7/2\}$	11330621	0.352
$3s 3p_{3/2} 3d_{3/2}\{3/2\}$	11582898	0.127
$3s 3p_{3/2} 3d_{3/2}\{5/2\}$	11686162	0.110
$3s 3p_{3/2} 3d_{3/2}\{1/2\}$	11739616	0.099
$3s 3p_{3/2} 3d_{5/2}\{9/2\}$	11983999	1800
$3s 3p_{3/2} 3d_{5/2}\{5/2\}$	12180192	0.812

rate as that of the $3s3p\ ^3\mathrm{P}_0^\mathrm{o}$ level would make little in the overall budget of the $3s3p\ ^3\mathrm{P}_2^\mathrm{o}$ level decays (Tab. 4).

4.4 Al-like ions

There are very few high-accuracy calculations on Al-like high-Z ions. The correlation corrections usually are small for very high-Z ions, but Breit interaction corrections along with the Lamb shift are very important. Huang included in his study [65] both Breit corrections and Lamb shifts. However, the Breit interaction was accounted for in the zero-frequency approximation. Beck and Norquist [66] performed medium-scale relativistic configuration interaction (RCI) calculations on Br^{22+} and Au^{66+}, including

Breit corrections and the Lamb shift. Safronova et al. [67] performed second-order relativistic MBPT calculations of the term energies in aluminum like ions. In this study, the numerical values were presented only for ions with nuclear charge $Z \le 42$. However, there also is a list of the strongest Au^{66+} E1 soft-X-ray lines. While MBPT and MR-MP used different zero-order approximations, the term energies and decay wavelengths are in perfect agreement with each other. Our calculational results on Al-like ions are given in Table 5. The entries for Al-like Au in Table 4 reveal that the lowest $J = 3/2$ level has two decay branches of about equal probability; one of these is the M1 decay to the ground state, the other would in LS-coupling be called an intercombination transition to the lowest quartet level. The fine structure intervals of the $3s^2 3p\ ^2\mathrm{P}^\mathrm{o}$ and $3s3p^2\ ^4\mathrm{P}$ terms are so large (at high Z) that the level multiplets overlap and the level sequence markedly differs from that at low nuclear charge.

Table 6. Second-order MR-MP transition probabilites of the forbidden M1/M2 and E2/E3 decays of the $3s3p3d$ $^4\mathrm{F}^o_{9/2}$ level in Al-like Au ions. The notation of the transition probabilities like $a(b)$ refers to $a \times 10^b\,\mathrm{s}^{-1}$; * denotes odd parity levels.

Lower levels	λ (Å)	type	A (s^{-1})
7/2(1)*	26.9847	M1	5.35(8)
		E2	5.90(6)
7/2(2)*	153.051	M1	3.12(6)
		E2	2.30(2)
5/2(1)*	21.1389	E2	1.21(4)
5/2(1)*	26.0746	E2	1.13(7)
5/2(1)*	27.6413	E2	1.03(6)
5/2(1)*	102.129	E2	1.38(2)
5/2(1)*	149.306	E2	1.156(2)
5/2(1)*	335.754	E2	1.55(−1)
5/2(1)	15.2075	M2	7.56(5)
		E3	2.51(3)
5/2(2)	19.5996	M2	5.81(5)
		E3	1.78(1)
5/2(3)	38.1173	M2	1.64(4)
		E3	8.30(0)
5/2(4)	49.3477	M2	3.11(1)
		E3	4.95(−4)
3/2(1)	14.8440	E3	5.80(3)
3/2(2)	15.6311	E3	1.63(2)
3/2(3)	16.9049	E3	6.26(−1)
3/2(4)	32.7032	E3	1.56(−3)
3/2(5)	44.7844	E3	3.13(−1)
τ (ps)			1797

Table 7. MR-MP calculated term values E (cm^{-1}) and lifetimes τ in Si-like gold ions. Lifetimes were evaluated by first-order wavefunctions.

State	E (cm^{-1})	τ (ps)
$3s^2 3p^2_{1/2}\{0\}$	0	
$3s^2 3p_{1/2}3p_{3/2}\{1\}$	3868416	1470
$3s^2 3p_{1/2}3p_{3/2}\{2\}$	3948550	62600
$3s3p^2_{1/2}3p_{3/2}\{2\}$	5384736	30.2
$3s3p^2_{1/2}3p_{3/2}\{1\}$	5620253	0.911
$3s^2 3p_{1/2}3d_{3/2}\{2\}$	5797009	77.8
$3s^2 3p_{1/2}3d_{3/2}\{1\}$	6190465	0.120
$3s^2 3p_{1/2}3d_{5/2}\{2\}$	6857655	2.15
$3s^2 3p_{1/2}3d_{5/2}\{3\}$	6870368	3.19
$3s3p^2_{1/2}3d_{3/2}\{1\}$	7351155	14.4
$3s3p^2_{1/2}3d_{3/2}\{2\}$	7416175	15.1
$3s^2 3p^2_{3/2}\{2\}$	7880660	399
$3s^2 3p^2_{3/2}\{0\}$	8058298	823
$3s3p^2_{1/2}3d_{5/2}\{3\}$	8369160	2.89
$3s3p^2_{1/2}3d_{5/2}\{2\}$	8491532	2.63
$3s3p_{1/2}3p^2_{3/2}\{2\}$	9168104	1.12
$3s3p_{1/2}3p^2_{3/2}\{3\}$	9333910	1.65
$3s3p_{1/2}3p^2_{3/2}\{0\}$	9430876	0.974

The transition rates of the many decay branches of the exceptionally long-lived $J = 9/2$ level ($3s3p3d$ $^4\mathrm{F}^o_{9/2}$ in LS coupling) are listed in Table 6. Such long-lived levels need to be taken into account in the modeling of plasmas and charge state distributions, because they feature time constants that are different from the bulk of the other levels and may be different from that of transient phenomena as experienced in laser fusion experiments.

Experimental data on Al-like ions up to Mo ($Z = 42$) have been compiled and systematized by Curtis and Jupén [68,69]. The results of our calculations on Xe ($Z = 54$) agree with the reanalyzed beam-foil data on this ion [15], lending support on the applicability of the calculational approach also to Au.

4.5 Si-like ions

The structure of Si-like ions up to $Z = 92$ as well as transitions between low-lying levels have been calculated by Huang [70] using the MCDF approach. Highly-correlated theoretical methods have been used only rarely. We have performed very accurate MR-MP calculations on a few low-energy levels in selected Si-like ions [71]. Those calculations did not include frequency-dependent Breit corrections and used a zero-order approximation different from the present work. Our new results on Si-like Au ions are given in Table 7. Table 4 comprises the decay branches of several low-lying long-lived levels in Si-like Au ions.

Again, as in the Al-like ions, there is a high-J excited level with a particularly long lifetime, the (in LS coupling notation) $3s^2 3p3d$ $^3\mathrm{F}^o_4$ level. The decay rates from this level are listed in Table 8. Decays of this level have not been observed with individual spectral line identification in any Si-like ion. However, a broad-band observation at a heavy-ion storage ring has yielded a level lifetime value for Si-like Fe^{12+} ions [73], and the experimental finding is compatible with calculations that employ our present theoretical apparatus [71].

As with the isoelectronic sequences listed before, the experimental data base is poor in the upper half of the periodic table of the elements. Jupén et al. [74] have systematized the experimental data up to Mo ($Z = 42$). Träbert et al. [13,14] have tentatively identified the two decay branches of the lowest quintet level on Xe ($Z = 54$) and Au ($Z = 79$). Bengtsson et al. [75] claimed to have identified these transitions in several ions just below $Z = 54$, but the isoelectronic trend of their data was grossly deviant from the semiempirical analysis by Jupén et al. [74] and from any calculation [76]. A calculation by Ishikawa and Vilkas [71] has confirmed the overall trend of the old calculations by Huang (in contrast to Bengtsson et al.), but suggested that the tentative identifications for Xe (where one the candidate lines is from a different level in the same ion, and the quintet level decays are probably blended with lines of the Al-like ion [15]) and Au (see below) would not hold. Huang et al. (a different person from the other Huang) presented data on Rh ($Z = 45$) [77] and calculations in the same range [78] that are not far from the previously assumed isoelectronic trend (but the paper does not mention any QED contributions). Meanwhile our calculations have been instrumental in identifying the two transitions in questions with other lines in the beam-foil

Table 8. Second-order MR-MP transition probabilites of the forbidden M1/M2 and E2/E3 decays of the $3s^23p3d$ $^3F^o_4$ level in Si-like Au ions. The notation of the transition probabilities like $a(b)$ refers to $a \times 10^b\,\mathrm{s}^{-1}$; * denotes odd parity levels.

Lower levels	λ (Å)	type	A (s^{-1})
3(1)	43.4923	E1	6.87(8)
3(1)*	26.9847	M1	5.30(8)
		E2	6.08(6)
3(2)*	74.9342	M1	1.55(6)
		E2	2.46(2)
3(3)*	147.454	M1	2.86(6)
		E2	2.46(2)
2(1)*	18.9262	E2	2.38(6)
2(2)*	20.5280	E2	3.63(4)
2(3)*	26.2415	E2	1.03(7)
2(4)*	66.6528	E2	1.83(3)
2(5)*	90.0182	E2	4.29(1)
2(6)*	159.024	E2	6.36(1)
1(1)	14.7059	E3	5.89(3)
1(2)	30.1454	E3	8.53(−7)
2(1)	14.8813	M2	5.92(5)
		E3	3.17(3)
2(2)	30.7480	M2	2.33(1)
		E3	5.33(−2)
2(3)	35.8712	M2	2.46(4)
		E3	1.53(1)
2(4)	45.9372	M2	3.23(1)
		E3	2.52(−4)
3(1)	43.4923	M2	3.02(1)
		E3	1.18(−4)
τ (ps)			807

Table 9. MR-MP calculated term values E (cm^{-1}) and lifetimes τ in P-like gold ions. Lifetimes were evaluated by first-order wavefunctions. The notation $a(b)$ for τ means $a \times 10^b$.

State	E (cm^{-1})	τ (ps)
$3s^23p^2_{1/2}3p_{3/2}\{3/2\}$	0	
$3s^23p^2_{1/2}3d_{3/2}\{3/2\}$	2015058	66.1
$3s^23p^2_{1/2}3d_{5/2}\{5/2\}$	3021626	2.93
$3s^23p_{1/2}3p^2_{3/2}\{3/2\}$	3805881	4.73(5)
$3s^23p_{1/2}3p^2_{3/2}\{5/2\}$	3907069	3280
$3s^23p_{1/2}3p^2_{3/2}\{1/2\}$	4042490	1.71(5)
$3s3p^2_{1/2}3p^2_{3/2}\{5/2\}$	5370224	1.80
$3s3p^2_{1/2}3p^2_{3/2}\{3/2\}$	5623795	0.877
$3s3p^2_{1/2}3p^2_{3/2}\{1/2\}$	5647785	0.982
$3s^23p_{1/2}3p_{3/2}3d_{3/2}\{5/2\}$	5795762	94.3
$3s^23p_{1/2}3p_{3/2}3d_{3/2}\{1/2\}$	5826491	85.0
$3s^23p_{1/2}3p_{3/2}3d_{3/2}\{3/2\}$	5830172	1.85
$3s^23p_{1/2}3p_{3/2}3d_{3/2}\{7/2\}$	5902446	540
$3s^23p_{1/2}3p_{3/2}3d_{3/2}\{5/2\}$	6165209	0.187
$3s^23p_{1/2}3p_{3/2}3d_{3/2}\{1/2\}$	6260938	0.135
$3s^23p_{1/2}3p_{3/2}3d_{3/2}\{3/2\}$	6271905	0.093
$3s^23p_{1/2}3p_{3/2}3d_{5/2}\{7/2\}$	6685794	733
$3s^23p_{1/2}3p_{3/2}3d_{5/2}\{9/2\}$	6797325	

two (low-lying) excited levels. In lower-Z ions, two levels of this $3s^23p^23d$ configuration have a high total angular momentum ($J = 9/2$); this blocks any E1 decay channels and leaves only M1 and M2 channels etc., which makes the level lifetime stand out from the others. For P-like Au, only one $J = 9/2$ level remains long-lived, while the other decays much more quickly because of much higher transition energies.

5 Comparison of calculational findings with experimental data

From the discussion above, it appears that the beam-foil data on Au [13,14] — as limited as they are — are the most extensive data sets on $n = 3$ $\Delta n = 0$ transitions in any high-Z range element, and that our calculations on Au are the only consistent set that covers many charge states of a given element. The intercomparison of these two sets therefore dominates this section. The key parameters of lines expected in such beam-foil or other light source spectra are listed in Table 10. Corresponding synthetic spectra based on our calculations are used to facilitate visual comparisons with the experimental observations. Table 11 lists the results of the previous decay curve analyses of levels in highly charged Au ions [12–14], but now associates some of them with other levels.

The first of the beam-foil spectroscopic observations [13] was obtained with a single spectrometer setting, covering a section of the EUV spectrum from 50 to 70 Å. At the given ion beam energy, Na- and Mg-like Au ions were expected to dominate the spectrum. The spectra recorded at various foil positions (corresponding to different delays after excitation) showed two line-like

spectrum of Xe [15], so that the systematic extension to Au appears viable.

4.6 P-like ions

Apparently only a single calculation (by Huang [79]) has been published on the high-Z range of the P isoelectronic sequence. A line of P-like U has been observed (and identified on the basis of dedicated calculations) near a line of the Na-like ion in the spectrum of highly charged U ions from an electron beam ion trap [3], but there was no systematic study of P-like ions. Our results on P-like ions are given in Table 9. We note that among the levels with picosecond lifetimes there are several that have predicted lifetimes in the range of a few hundred nanoseconds, which is very long for such highly charged ions. Some details of the level structure are drastically different from the situation at lower nuclear charge (as given for the example of Cu^{14+} ions in [80]), and this is a result of the very large spin-orbit splitting at high Z, also considered as a regrouping of relativistic configurations [81]. In low-charge P-like ions, the $3s^23p^3$ ground configuration has 5 levels well below any other level. In Au^{64+}, one of them is far above all others that are listed in Table 9. Similarly, the group of $3s3p^4$ levels (low-lying 'displaced' terms at low Z) is broken up; moreover, two $3s^23p^23d$ levels are now the first

Table 10. Beam-foil spectrum of gold ions and line identifications from our calculations. The numbers refer to spectral features in Figure 3 and in adjacent spectra (not shown). Experimental wavelength uncertainties are about 0.3 Å. The elemental symbols Na, Mg, Al, Si and P denote the isoelectronic sequences. A is the full decay probability; $A^2\tau$ the same but weighted for the branching fraction of the given transition. The notation $a(b)$ for τ means $a \times 10^b$.

No	λ_{expt}	λ_{theor}	Upper state	τ (ps)	Lower state	A (s^{-1})	$A^2\tau$	Seq.
1	61.13	60.994	$3p_{1/2}3d_{3/2}\{2\}$	16.68	$3p_{1/2}3p_{3/2}\{2\}$	3.10(10)	1.60(10)	Mg
2	62.64	62.949	$3p_{1/2}^2\{0\}$	6.81	$3s_{1/2}3p_{3/2}\{1\}$	1.47(11)	1.47(11)	Mg
3	64.37	64.344	$3s3p_{1/2}^23d_{3/2}\{1\}$	14.39	$3s^23p_{1/2}3d_{3/2}\{2\}$	4.26(10)	2.61(10)	Si
4	64.83	64.771	$3s3p_{1/2}^23p_{3/2}3d_{5/2}\{7/2\}$	16.07	$3s^23p_{1/2}3p_{3/2}3d_{3/2}\{7/2\}$	1.86(10)	1.86(10)	P
5	65.93	65.949	$3s3p_{1/2}^23p_{3/2}\{2\}$	30.23	$3s^23p_{1/2}3p_{3/2}\{1\}$	1.83(10)	1.01(10)	Si
6	66.65	66.461	$3s3p_{1/2}^2\{1/2\}$	21.50	$3s^23p_{1/2}\{1/2\}$	4.65(10)	4.65(10)	Al
7	69.70	69.629	$3s3p_{1/2}^23p_{3/2}\{2\}$	30.23	$3s^23p_{1/2}3p_{3/2}\{2\}$	1.48(10)	6.59(09)	Si
8	69.96	70.009	$3p_{1/2}\{1/2\}$	20.20	$3s_{1/2}\{1/2\}$	4.95(10)	4.95(9)	Na
9	71.77	71.670	$3s3p_{1/2}3p_{3/2}\{5/2\}$	58.7	$3s^23p_{3/2}\{3/2\}$	1.70(10)	1.70(10)	Al
		71.846	$3s3p_{3/2}\{1\}$	45.65	$3s^2\{0\}$	2.19(10)	2.19(10)	Mg
10	73.0	72.950	$3s3p_{1/2}3d_{3/2}\{3/2\}$	5.00	$3s3p_{1/2}^2\{1/2\}$	4.87(9)	1.19(8)	Al
10	73.0	73.009	$3p_{1/2}^23d_{3/2}\{3/2\}$	5.44	$3s3p_{1/2}3d_{3/2}\{3/2\}$	1.09(10)	6.50(8)	Al
		74.212	$3p_{1/2}3d_{3/2}\{2\}$	16.68	$3s3d_{3/2}\{1\}$	2.08(10)	7.23(9)	Mg
		74.355	$2p_{3/2}^{-1}3p_{1/2}\{2\}$	24.86	$2p_{3/2}^{-1}3s\{2\}$	2.02(10)	1.10(10)	Ne
11	74.9	74.995	$2p_{3/2}^{-1}3p_{1/2}\{1\}$	24.14	$2p_{3/2}^{-1}3s\{2\}$	3.33(10)	2.89(10)	Ne
12	75.8							
13	77.5	77.439	$2p_{1/2}^{-1}3p_{1/2}\{1\}$	19.16	$2p_{1/2}^{-1}3s\{0\}$	1.18(10)	2.79(9)	Ne
14	78.5	78.734	$2p_{3/2}^{-1}3p_{1/2}\{2\}$	24.86	$2p_{3/2}^{-1}3s\{1\}$	1.71(10)	7.82(9)	Ne
14	78.5	79.094	$2p_{1/2}^{-1}3p_{1/2}\{1\}$	19.16	$2p_{1/2}^{-1}3s\{1\}$	2.17(10)	9.38(9)	Ne
		79.453	$2p_{3/2}^{-1}3p_{1/2}\{1\}$	24.14	$2p_{3/2}^{-1}3s\{1\}$	5.04(9)	6.63(8)	Ne
15	80.3	79.546	$3s3p_{1/2}3p_{3/2}3d_{3/2}\{4\}$	24.20	$3s^23p_{3/2}3d_{3/2}\{3\}$	1.18(10)	3.39(9)	Si
15	80.3	80.720	$4(2)$	61.69	$4(1)^*$	3.53(9)	7.68(8)	Si
15	80.3	81.020	$3s3p_{1/2}3p_{3/2}\{3/2\}$	41.53	$3s^23p_{3/2}\{3/2\}$	2.38(9)	2.35(8)	Al
15	80.3	81.585	$3s3p_{1/2}^23d_{3/2}\{2\}$	15.06	$3s^23p_{1/2}3d_{1/2}\{1\}$	9.08(10)	1.24(9)	Si
		81.693	$3p_{1/2}3d_{3/2}\{2\}$	16.68	$3s3d_{3/2}\{2\}$	6.82(9)	7.75(8)	Mg
		84.310	$5/2(8)$	7.41	$3/2(6)^*$	8.13(9)	4.90(8)	P
16	83.0	84.400	$3s3p_{1/2}3d_{3/2}\{5/2\}$	18.01	$3s^23d_{3/2}\{3/2\}$	9.85(10)	2.86(9)	Al

Table 11. Comparison of the calculated E1 lifetimes with the results of lifetime measurements [13,14] after the re-assignment of spectral lines.

Upper level	Lower level	λ (Å) This work	τ (ps) This work	λ (Å) Other	τ (ps) Other	τ (ps) Experiment
Na-like						
$3p_{1/2}$ $^2P^o_{1/2}$	$3s$ $^2S_{1/2}$	70.009	20.20	69.974[a]		25±5 [f]
Mg-like						
$3s3p_{3/2}$ $^3P^o_1$	$3s^2$ $^1S_0$	71.846	45.65	71.806[b]		18±4 [f] blended 50.5±2 [g,h] blended Al
Al-like						
$3s3p_{1/2}^2$ $^4P_{1/2}$	$3s^23p_{1/2}$ $^2P_{1/2}$	66.461	21.50	65.25[c] 66.09[d]	17.8[c]	22±4 [g]
$3s3p_{1/2}3p_{3/2}$ $^4P_{5/2}$	$3s^23p_{3/2}$ $^2P_{3/2}$	71.670	58.70	69.83[c] 71.66[d]	53.2[c]	50.5±4 [g,h] blended Mg
$3s3p_{1/2}3p_{3/2}$ $^4P_{3/2}$	$3s^23p_{3/2}$ $^2P_{3/2}$	81.020	41.43	78.86[c]	37[c]	
Si-like						
$3s3p^3$ $^5S^o_2$	$3s^23p^2$ $^3P_1$	65.949	30.23	64.83[e]	27.7[e]	31±5 [g]
$3s3p^3$ $^5S^o_2$	$3s^23p^2$ $^3P_2$	69.629	30.23	68.40[e]	27.7[e]	37±7 [g]

[a] MCDF+QED calculation, reference [7]; [b] MBPT calculations, reference [63]; [c] MCDF calculations by Huang [65]; [d] RCI calculations by Beck and Norquist [66]; [e] MCDF calculations by Huang [70]; [f] [13]; [g] [14]; [h] previous lifetime error bar doubled in recognition of line blend.

humps and a number of weaker features that blended into wide spectral structures, leaving much of the analysis to interpretation. The radiative lifetime measurement of the line that was assumed to represent the lowest $J = 1$ level in the Mg-like ion (intercombination transition) differed significantly from expectation.

The second measurement campaign [14] used an ion beam energy that was a little lower, so that Na-like ions were no longer expected to be seen; it was assumed at the time that no lines from Mg-like ions were seen either. The dominant spectral feature was a line then identified with a candidate transition in Al-like Au ions; most of the many weak spectral features in the wavelength range 110 to 170 Å (observation in second diffraction order of the wavelength range of the first campaign, for the benefit of much better spectral resolution) remained unidentified.

Wavelength and lifetime data for one of the levels in Al-like Au have since been questioned on the basis of specific calculations [66]. In the following, we re-analyse the raw data of both beam-foil experiments in the light of our present calculations and take into account insights from our corresponding work on Xe; this process includes improvements of the original wavelength calibrations.

Both of the earlier beam-foil experiments were aimed primarily at lifetime measurements; at the time it was assumed sufficient to establish an approximate wavelength calibration. The experimental set-up of the beam-foil work on Au has been described elsewhere [12–14]. The EUV spectrometer at the Unilac accelerator of GSI Darmstadt could be rotated and swiveled in its vacuum tank, so that one could position the optical axis at right angles to the ion beam. Opposite the spectrometer entrance slit (that faced the ion beam at a close distance) was a Penning discharge lamp that provided a stationary light source for *in situ* calibration. The stationary light source calibration was transferred to the spectra from the fast ion beam (which are notably Doppler shifted) by ways of careful control of the observation geometry and a separate measurement of the ion velocity. The Penning lamp, however, provided a very limited number of well-defined lines in the EUV (of Ne and Al [82]), and only at wavelengths longer than 130 Å. Evidently, this was far away from the operating range in the first campaign, and it was one of the reasons for changing to higher-diffraction order (second, third, and fourth) observation in the second campaign. However, it was not possible to find sufficiently many calibration lines that would be covered in a given setting of the position sensitive photon detector, and the dispersion was established only approximately. This shortcoming was made worse by the need to exploit the full width of the detector in order to cover a sufficiently wide wavelength range and number of lines of interest in the allocated accelerator time; many such a detector with a position evaluation read-out that depends on charge or voltage ratios is fairly linear only near the center, in perhaps 50% of its full width. As a consequence, the measurement conditions in the Au experiments were not suitable for reliable wavelength determinations. We now apply a more sensible theoretical calibration curve with a sliding dispersion scale

rather than the constant dispersion within each spectral exposure that was used previously, but this is not sufficient to provide wavelength data of higher precision. The improvement resides mostly in the internal consistency of the revised line identifications.

If the exciter foil is sufficiently thick (still rather thin in absolute terms), the charge state distribution reaches an equilibrium. The background level as well as the range of charge states in a beam-foil spectrum can be reduced by using a thick foil well upstream of the observation zone, separating the charge states in a magnetic field, and letting a selected single-charge state ion beam pick up electrons in a thin foil, after which observation takes place. The top two spectra in Figure 2 illustrate the difference. Because of the reduced ion beam current in the second option, the overall signal drops accordingly (see the y-axis scales of the figures) and renders such a procedure very time-consuming, but the spectra are notably cleaner. Without systematic survey spectra at various ion beam energies (which would have required much more machine time and considerable operator effort), the charge state distribution of the emerging ion beam in the GSI experiment remained insufficiently well known. The present re-analysis and new line identification yields such information, but only a long time after the event.

Figure 2 shows recalibrated data from the first beam-foil spectroscopy campaign [12,13], as well as a new composite spectrum constructed from data gathered during the second such campaign [14]. There are several key changes from the earlier presentations of these data, as is detailed in the following. The wavelength scale of the spectra of the first campaign (using an ion beam of energy 13.2 MeV/amu) was tied to a line that was identified with the $3s\ ^2S_{1/2}$ - $3p\ ^2P^o_{1/2}$ transition in Na-like Au and its calculated wavelength of 69.97 Å [7]. The reliability of that calculation has since been corroborated [2,3,5]. Such resonance lines in Na-like ions are usually among the brightest in beam-foil spectra, and it was assumed that the brightest line in the Au spectrum, at a position close to the expected one, was indeed from this transition.

Close to this line, a similar $3s$ - $3p_{1/2}$ transition is expected to give rise to the $3s^2\ ^1S_0$ - $3s3p\ ^3P^o_1$ transition in the Mg-like ion. The calculations by Cheng and Johnson [29] for this transition in Mg-like ions do not cover all elements and thus necessitate interpolation over wide gaps. The calculational results obtained by Ivanova et al. [30] differ significantly from those of Cheng and Johnson for high Z. The differences amount to up to 1.5% at $Z = 92$ (see Fig. 1). This is more than the typical wavelength difference between lines in the spectra of high-Z elements. A third set of calculations [31] was available, but was not recognized as such, because it mainly presented information on hyperfine interaction effects. The results of this calculation are closer to those obtained by Ivanova et al. (but majority vote among calculations is not a recognized measure of quality). A fourth calculation of Mg-like ions [32] has been published since. The results for the $3s3p\ ^{1,3}P^o_1$ levels along the isoelectronic sequence are shown in Figure 1. Because one set of predictions [31]
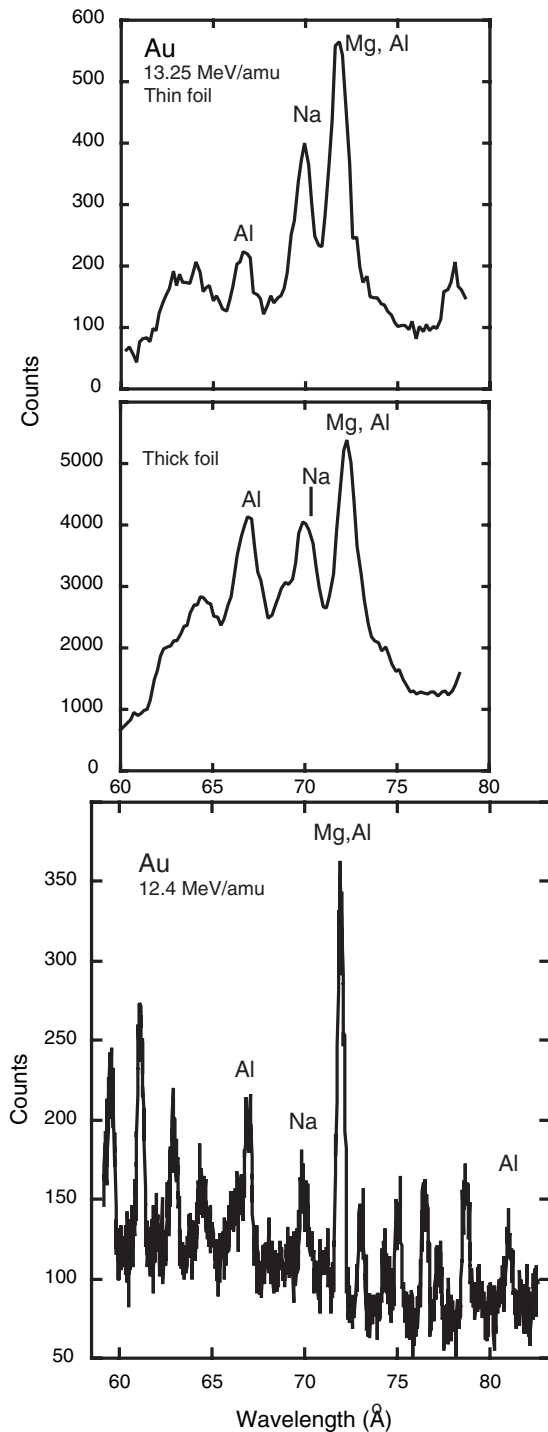
Fig. 2. Three samples of Au spectra after beam-foil excitation of 13.25 MeV/amu and 12.4 MeV/amu Au ion beams (replotted data of [13,14]). Na, Mg, and Al denote the isoelectronic sequences of the corresponding Au lines. All spectra are accumulated from spectra recorded at different positions of the exciter foil and therefore at different delay times after excitation. The bottom spectrum furthermore is a composite of several such accumulated spectra that were recorded in second diffraction order (apparent wavelength range some 120 to 170 Å) but scaled in wavelength to match the other spectra. The spectral lines that are not recognizable or not covered in the first-order observations probably belong to the longer-wavelength range.

covers the most elements, we show the differences of the other three calculations from this one. Evidently, for both levels the calculations by Cheng and Johnson [29] predict the highest level energies at high Z. For the singlet level, the calculation by Ivanova et al. [30] matches the experimental data (which are available only in the lower half of the isoelectronic sequence) best and remains close in trend to the reference values. Unfortunately, this does not guarantee that either of them is valid at high Z. For the triplet level, the calculations by Ivanova et al. and by Zou and Froese Fischer [32] are close to the experimental data at rather low Z, but their trends begin to differ significantly at medium Z. Again, this gives no proper clue for the high-Z behaviour.

What should at the time have been considered a clue to the analysis of the beam-foil spectra is that the energy of the triplet level of the Mg-like ion very likely remains lower than that of the $3p_{1/2}$ level along the isoelectronic sequence. This rule-of-thumb contradicts the line identification made in the beam foil work on Au (guided perhaps too much by reference to [29]), favouring instead the trend of the predictions by Ivanova et al. [30] and by Marques et al. [31]. For two lines in the spectrum therefore the classifications need to be interchanged; the other line being a wavelength reference from the Na-like ion. Figure 2 reflects this interchange. The line from the Na-like ion is no longer associated with the strongest line in the spectrum — nor does the Mg-like ion on its own explain it. Instead, the present calculations indicate that the strongest line has to be attributed to a close blend of two prominent lines from two different charge state ions (see below). Such a prediction can reliably be made only by calculations that treat different ions with the same formalism and detail (as was done here, but was not available before).

The spectrometer performance was notably improved between the two measurement campaigns on Au [12–14], and we discuss as an example mostly the data from the latter effort. Composite spectra combined from delayed spectra recorded in the second campaign are shown in Figures 2 and 3. The corresponding wavelength, transition probability, and level lifetime values are listed in Table 10. In the earlier work [14], the data now shown in the bottom spectrum of Figure 2 and in Figure 3 have been presented with the apparent wavelength scale of observation in second diffraction order. Several of the lines that appear outside of the range of the early (first diffraction order) observations may actually belong to the long-wavelength range. Several of those lines coincide in wavelength with decay branches of the particularly long-lived high-J levels in Al- and Si-like Au ions. However, the calculated lifetimes and small branch fractions make observation of these decays unlikely under the given conditions of the beam-foil experiment.

One line dominates the spectra in Figure 2. In the first campaign, the line was observed in first diffraction order, without any nearby calibration line; in the second campaign observation was mainly in second order of diffraction. However, third and fourth diffraction order images of the same line were then compared to calibration lines
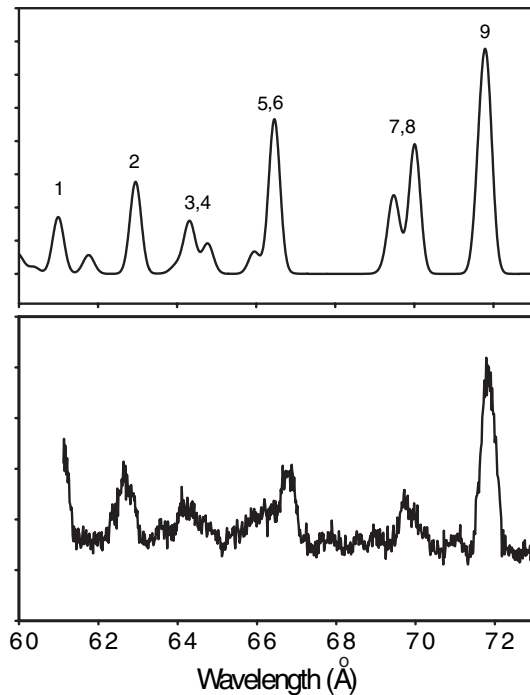
Fig. 3. Synthetic spectra of Ne-like, Na-like, Mg-like, Al-like, Si-like and P-like gold ions in comparison to an experimental spectrum. The numeric labels in the synthetic spectrum identify specific transitions in table 10. The assumed abundance of ions of different charge states is 0.09 for Ne-like ions, 0.15 Na, 0.25 Mg, 0.18 Al, 0.09 Si, and 0.05 P. Decay branching was accounted for. The spectrum was simulated for a delay time of 20 ps. The wavelength of the strongest line was 'calibrated' to 71.77 Å — the average of two theoretical lines: Mg 71.670 Å and Al 71.846 Å. The experimental spectrum (a section of Fig. 2) was shifted by 0.134 Å from its 71.8 Å wavelength reference. Due to the line blend in the reference line, the calibration may have a 0.1 Å error.

Fig. 4. Isoelectronic trend of the scaled line strength S for the intercombination transition in Mg-like ions. In this presentation, the three wide-range calculations by Cheng and Johnson [29] (full line), by Huang and Johnson [86] (long dash broken line, only in the lower Z part), and by Zou and Froese Fischer [32] (broken line) largely agree with each other (details of the low-Z range have been discussed elsewhere [87]). Most experimental data (full dots) ([13,15,88–93] and this work) are compatible with the predicted trend. The error bars for Xe ($Z = 54$) and Au ($Z = 79$) appear particularly large because of the scaling; in both ions, the decay curves have been obtained on line blends of Mg- and Al-like ions. An exception to the overall gross agreement of theory and experiment are the medium-high Z data reported by Hutton [94] (full squares), which are given with rather small error bars, but which describe a systematically different trend that has not been fully understood yet.

from a stationary light source. This line is the key to all of the spectral re-analysis of the beam-foil data mentioned above.

Irritatingly, a crude estimate in the laboratory notes during the accelerator run gave a wavelength of 71.8 Å (which in hindsight seems near perfect), whereas two detailed later evaluations resulted in a wavelength value of 72.7 Å which was adopted previously. However, the difference between these two values coincides with the magnitude of the second order Doppler effect, and communication errors may have been the cause for the incidental adoption of the reference value from the stationary calibration instead of the value corrected for observation of a fast ion light source. This line then is the same blend of Mg- and Al-like ion lines as mentioned above from the re-investigation of the first campaign, only the relative contributions from the two ion species must favour the Al-like ion in the second campaign (shift of the charge state distribution because of the lower ion beam energy). While originally it was claimed that at the ion beam energy of the second campaign no light from Mg-like ions was seen (looking at the wrong line position), the new interpreta-
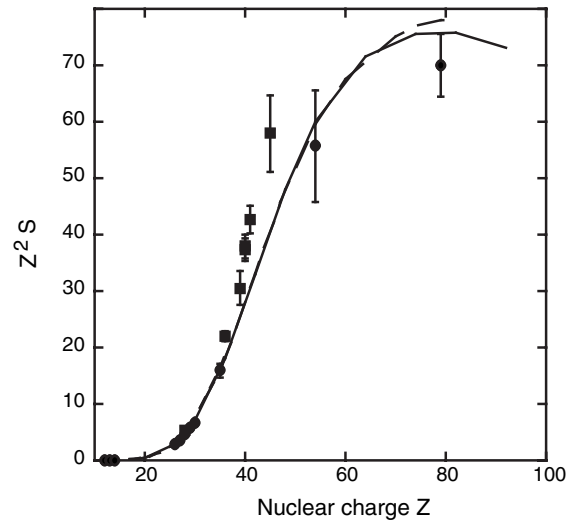
tion of the same data assumes that the signature line from the Au^{67+} $3s3p$ ^{3}P$_1^o$ level decay is part of a close blend with the equally prominent Au^{66+} $3s3p^2$ ^{4}P$_{5/2}$ level decay; the blend is so close that spectral fitting is not sufficient to quantify the admixture. However, the synthetic spectra are based on a charge state distribution that includes the Mg-like ion charge state as the highest; as expected, the signature line of the Na-like ion is much reduced (Fig. 3) at the lower ion beam energy (12.4 MeV/amu).

The decay curve of this strong line [14] would then reflect a superposition of two decay curves of neighbouring ion charge states. Incidentally, the predictions for both level lifetimes are rather close to each other. The lifetime result obtained on the blend (about 50 ps) is about the mean of both predictions (of about 46 ps and 59 ps for the Mg-like and Al-like ion levels, respectively). Now realizing that the decay curve represents two decays of rather similar time constants that cannot be disentangled by multi-exponential fits, we have doubled the error estimate on the lifetime result of a single representative fit component. At about 8% uncertainty, the lifetime value of this representative 'effective' exponential is compatible with either of the two expected contributors. Figure 4 shows this result in the isoelectronic trend of the Mg

sequence. The present re-interpretation of the data would resolve the lifetime discrepancy for Au^{67+} stated in [13] (decay curve of the wrong line). Beck and Norquist [66] have claimed an error in the lifetime determination of the Au^{66+} $J = 5/2$ level in reference [14]; the now recognized line blend with the Au^{67+} line explains why the experiment did not match their expectation. Of course, two lifetimes so close to each other cannot be resolved from each other by multi-exponential fitting. The lifetime values reported in [12–14], however, bear error bars that are larger than the statistical uncertainties because of various systematic error problems discussed in those papers, and thus the quoted lifetime values remain good estimates for each of the two ions and levels involved.

Table 11 comprises the results of level lifetime measurements on Na- through Si-like ions of Au. The listing indicates that there is no discrepancy of present lifetime prediction and previous measurement now that several lines have been reassigned. The earlier result of about 18 ps (with an uncertainty of more than 20%) for the (misidentified) intercombination line in the Mg-like Au ion may reflect the presence of another short-lived line blend, or it may result from a misinterpretation of multi-exponential fit results that sometimes show several alternatives, none of which is of superior merit on statistical grounds alone. On the other hand, some of the old lifetime results for then thought to be unrelated lines now corroborate the new insight from structure calculations as to which lines represent the two decay channels of the lowest quintet level in the Si-like Au ion.

6 Discussion and conclusions

Some ten years after the fast-ion beam measurements on highly charged Au ions and some five years after corresponding electron beam ion trap (EBIT) measurements [83], computations have remarkably improved. They supersede some earlier theoretical work that had served as guidance for the spectral analysis of data far beyond the range of nuclear charge Z for which a fairly consolidated body of atomic data existed at the time. In the light of the new calculations, some earlier line identifications in the beam-foil spectra of highly charged Au ions have been re-investigated and partly revised. In several cases, the modern calculations enable immediate line identifications, the experimental wavelengths in turn providing feedback on the quality of the calculations. A fruitful interplay of experiment and theory is now becoming possible.

A decisive path towards establishing unequivocal line assignments (and to cover more than just a few key decays of a few low-lying levels) would require systematic studies, with well resolved spectral observations for a fair number of ion species between Xe ($Z = 54$) and Au ($Z = 79$). These spectra would need to be correlated by suitable atomic structure calculations in order to ascertain line identities and to control the validity of the calculations for interpolations of the data. Considering the scarcity of suitable heavy-ion accelerators, the experimental task will

probably fall to other devices, most likely to electron beam ion traps. Those electron beam ion traps, however, show significantly different spectra [83] because of their low density operation (and dominant excitation from the ground state) in contrast to the high density excitation in beam-foil spectroscopy. The three lines from highly charged Au ions that were seen in the EBIT spectra corroborate the results of the present Multi-Reference Møller-Plesset calculations to within better than 0.1 Å.

One of the unique advantages of the beam-foil light source lies in the fact that it inherently provides time resolution and thus can be used to determine atomic level lifetimes in the picosecond- to nanosecond-range. The revised line assignment for the Mg-like Au ion intercombination line removes any discrepancy between lifetime prediction and measurement for the $3s3p$ $^3P_1^o$ level of this ion. An alternative suggestion [66] to explain the mild discrepancy of the experimental findings for an intercombination line of the Al-like ion Au^{66+} with the lifetime prediction (now identified as a previously unrecognized spectral line blend) called for satellite line contamination. In a similar vein, for some lighter ions in somewhat lower charge states, an ion-energy variation resulted in significantly different lifetime results [85], which was interpreted as also pointing at the problem of satellite line contamination (if the ion beam energy is chosen much below the optimum production value). The presently reevaluated data show no sign of either. A systematic offset between lifetime prediction and measurement that has been observed in medium-Z Mg-like ions in beam-foil experiments at the RIKEN accelerator [84] is not corroborated by either the GSI work on Xe [12,15] or the present work on Au. The data from RIKEN, with their striking internal consistency and small error bars line out an isoelectronic trend that so far defies any theoretical model.

The present Multi-Reference Møller-Plesset calculations have been applied in a way that is non-traditional for spectroscopy. Not one single atomic system has been calculated for various nuclear charges, but various charge state ions of a given element. This reflects the situation in any given spectroscopic observation. Only by applying the same high-level calculational apparatus to various ion species becomes the intercomparison of the predicted line spectra immediately meaningful. Systematic errors of the calculation have a good chance to cancel in such a comparison. The accuracy of the calculational scheme is of high importance; here we see that the present calculations of transition energies in Na-like ions come close to some of the very best. On comparable ions with more than a single valence electron [11], the same type of calculation has fared equally well. For the practical use of synthetic spectra not only transition energies, but also transition rates and branch fractions are wanted; the resulting spectra, modulated by the experimental charge state distribution, provide a valid visual impression that is very valuable for the comparison with experimental observations, in particular for the cross-checking of lines for completeness of the line catalogue, for spectral blends, or foreign contaminants. Taking the transition rates into account makes it

possible to discriminate between prompt and delayed spectra even by means of synthetic spectra (the cascade repopulation process is another massive calculational effort not tried here), or the very different appearance of spectra under high- or low-density excitation conditions.

There is much more work that needs to be done before truly complex and line-rich spectra can be understood in sufficient detail by reliable calculations. As an example of the challenges lying ahead we like to point out the EUV spectra of heavy elements (for more details and references see [95]) that were obtained of some fusion test plasmas at Oak Ridge and foil-excited ion beams at Brookhaven and that at the time were suspected to originate from Pm-like ions (61 electrons in total, of which very few reside outside a very-many electron core). An attempt to clarify the situation by beam-foil spectroscopy of Au and neighbouring elements at Bochum [95] gave little support to the earlier hypotheses, but the Bochum beam-foil spectra of their own showed a high number of lines that for lack of accurate calculations had to remain unclassified. The present calculational effort with its accurate results has demonstrated what can be achieved for the spectra of multi-electron high-Z ions at medium to high ion charges, and the comparison with experimental data validates the present computational technique as a major stepping stone on the path towards understanding even more complex spectra.

References

1. E. Träbert, P. Beiersdorfer, J.K. Lepson, H. Chen, Phys. Rev. A **68**, 042501 (2003)
2. P. Beiersdorfer, H. Chen, D.B. Thorn, E. Träbert, Phys. Rev. Lett. **95**, 233003 (2005)
3. P. Beiersdorfer, E. Träbert, H. Chen, M.-H. Chen, M.J. May, A.L. Osterheld, Phys. Rev. A **67**, 052103 (2003)
4. S.B. Utter, P. Beiersdorfer, E. Träbert, E.J. Clothiaux, Phys. Rev. A **67**, 032502 (2003)
5. E. Träbert, P. Beiersdorfer, H. Chen, Phys. Rev. A **70**, 032506 (2004)
6. W.R. Johnson, S.A. Blundell, J. Sapirstein, Phys. Rev. A **38**, 2699 (1988)
7. Y.-K. Kim, D.H. Baik, P. Indelicato, J.P. Desclaux, Phys. Rev. A **44**, 148 (1991)
8. S.A. Blundell, Phys. Rev. A **47**, 1790 (1993)
9. S.B. Utter, P. Beiersdorfer, E. Träbert, Can. J. Phys. **81**, 911 (2003)
10. E. Träbert, P. Beiersdorfer, K.B. Fournier, M.H. Chen, Can. J. Phys. **83**, 829 (2005)
11. M.J. Vilkas, Y. Ishikawa, Phys. Rev. A **72**, 032512 (2005)
12. E. Träbert, J. Doerfert, J. Granzow, R. Büttner, U. Staude, K.-H. Schartner, P. Rymuza, P.H. Mokler, L. Engström, R. Hutton, Phys. Lett. A **188**, 355 (1994)
13. E. Träbert, J. Doerfert, J. Granzow, R. Büttner, U. Staude, K.-H. Schartner, P. Rymuza, L. Engström, R. Hutton, Z. Phys. D **32**, 295 (1995)
14. E. Träbert, U. Staude, P. Bosselmann, K.-H. Schartner, P.H. Mokler, X. Tordoir, Eur. Phys. J. D **2**, 117 (1998)
15. J.R. Vilkas, Y. Ishikawa, E. Träbert, J. Phys. B: At. Mol. Opt. Phys. **39**, 2195 (2006)
16. Y.-K. Kim, Phys. Scripta T **73**, 19 (1997)
17. P. Beiersdorfer, S. von Goeler, M. Bitter, E. Hinnov, R. Bell, S. Bernabei, J. Felt, K.W. Hill, R. Hulse, J. Stevens, S. Suckewer, J. Timberlake, A. Wouters, M.H. Chen, J.H. Scofield, D.D. Dietrich, M. Gerassimenko, E. Silver, R.S. Walling, P.L. Hagelstein, Phys. Rev. A **37**, 4153 (1988)
18. J.F. Seely, R.A. Wagner, Phys. Rev. A **41**, 5246 (1990)
19. P. Beiersdorfer, J. Nilsen, J.H. Scofield, M. Bitter, S. von Goeler, K.W. Hill, Phys. Scripta **51**, 322 (1995)
20. J.F. Seely, U. Feldman, C.M. Brown, D.D. Dietrich, W.E. Behring, J. Opt. Soc. Am. B **5**, 785 (1988)
21. J.F. Seely, C.M. Brown, U. Feldman, J.O. Ekberg, C.J. Keane, B.J. MacGowan, D.R. Kania, W.E. Behring, At. Data Nucl. Data Tab. **47**, 1 (1991)
22. H. Gould, Nucl. Instrum. Meth. B **9**, 658 (1985)
23. R.E. Marrs, S.R. Elliott, D.A. Knapp, Phys. Rev. Lett. **72**, 4082 (1994)
24. T.E. Cowan, C. Bennett, D. Dietrich, J.V. Bixler, C.J. Hailey, J.R. Henderson, D.A. Knapp, M.A. Levine, R.E. Marrs, M.B. Schneider, Phys. Rev. Lett. **66**, 1150 (1991)
25. A. Simionovici, D.D. Dietrich, R. Keville, T. Cowan, P. Beiersdorfer, M.H. Chen, S.A. Blundell, Phys. Rev. A **48**, 3056 (1993)
26. P. Beiersdorfer, B.J. Wargelin, Rev. Sci. Instrum. **65**, 13 (1994)
27. I.P. Grant, B.J. McKenzie, P.H. Norrington, D.F. Mayers, N.C. Pyper, Comput. Phys. Commun. **21**, 207 (1980)
28. B.J. McKenzie, I.P. Grant, P.H. Norrington, Comput. Phys. Comm. **21**, 233 (1980)
29. K.T. Cheng, W.R. Johnson, Phys. Rev. A **16**, 263 (1977)
30. E.P. Ivanova, L.N. Ivanov, M.A. Tsirekidze, At. Data Nucl. Data Tab. **35**, 419 (1986)
31. J.P. Marques, F. Parente, P. Indelicato, At. Data Nucl. Data Tab. **55**, 157 (1993)
32. Y. Zou, C. Froese Fischer, J. Phys. B **34**, 915 (2001)
33. L.J. Curtis, P.S. Ramanujam, J. Opt. Soc. Am. **73**, 979 (1983)
34. J. Sucher, Phys. Rev. A **22**, 348 (1980)
35. M.H. Mittleman, Phys. Rev. A **24**, 1167 (1981)
36. M.J. Vilkas, Y. Ishikawa, Phys. Rev. A **72**, 032512 (2005)
37. M.J. Vilkas, Y. Ishikawa, K. Koc, Phys. Rev. E **58**, 5096 (1998)
38. I.M. Savukov, W.R. Johnson, Phys. Rev. A **65**, 042053 (2002)
39. C. Møller, M.S. Plesset, Phys. Rev. **46**, 618 (1934)
40. M.J. Vilkas, Y. Ishikawa, Phys. Rev. A **68**, 012503 (2003)
41. M.J. Vilkas, Y. Ishikawa, Phys. Rev. A **69**, 062503 (2004)
42. Y. Ishikawa, H.M. Quiney, G.L. Malli, Phys. Rev. A **43**, 3270 (1991)
43. P. Indelicato, O. Gorceix, J.P. Desclaux, J. Phys. B **20**, 651 (1987)
44. Y.-K. Kim, in *Atomic Processes in Plasmas* (AIP Conf. Proc. No. 206, 1990), p. 19

45. P.J. Mohr, Phys. Rev. A **46** 4421 (1992)
46. J.A. Cogordan, S. Lunell, Phys. Scripta **33**, 406 (1986)
47. P.L. Hagelstein, R.K. Jung, At. Data Nucl. Data Tab. **37**, 121 (1987)
48. H.L. Zhang, D.H. Sampson, At. Data Nucl. Data Tab. **43**, 1 (1989)
49. E.V. Aglitskii, E.P. Ivanova, U.I. Safronova, S.I. Ulityn, L.A. Vainshtein, J.-F. Wyart, Phys. Scripta **40**, 601 (1989)
50. L.A. Vainshtein, U.I. Safronova, At. Data Nucl. Data Tab. **21**, 49 (1978)
51. U.I. Safronova, A.S. Shlyaptseva, A.M. Urnov, J. Phys. B **14**, 1249 (1981)
52. E.P. Ivanova, A.V. Gulov, At. Data Nucl. Data Tab. **49**, 1 (1991)
53. P. Quinet, T. Gorlia, E. Biémont, Phys. Scripta **44**, 164 (1991)
54. U.I. Safronova, M.S. Safronova, R. Bruch, Phys. Scripta **49**, 446 (1994)
55. U.I. Safronova, C. Namba, I. Murakami, W.R. Johnson, M.S. Safronova, Phys. Rev. A **64**, 012507 (2001)
56. G.A. Chandler, M.H. Chen, D.D. Dietrich, P.O. Egan, K.P. Ziock, P.H. Mokler, S. Reusch, D.H.H. Hoffmann, Phys. Rev. A **39**, 565 (1989)
57. D.D. Dietrich, A. Simionovici, M.H. Chen, G. Chandler, C.J. Hailey, P.O. Egan, P.H. Mokler, S. Reusch, D.H.H. Hoffmann, Phys. Rev. A **41**, 1450 (1990)
58. P. Beiersdorfer, M.H. Chen, R.E. Marrs, M.A. Levine, Phys. Rev. A **41**, 3453 (1990)
59. W.R. Johnson, S.A. Blundell, J. Sapirstein, Phys. Rev. A **38**, 2699 (1988)
60. J. Reader, V. Kaufman, J. Sugar, J.O. Ekberg, U. Feldman, C.M. Brown, J.F. Seely, W.L. Rowan, J. Opt. Soc. Am. B **4**, 1821 (1987)
61. J.O. Ekberg, U. Feldman, J.F. Seely, C.M. Brown, Phys. Scripta **40**, 643 (1989)
62. J.O. Ekberg, U. Feldman, J.F. Seely, C.M. Brown, B.J. MacGowan, D.R. Kania, C.J. Keane, Phys. Scripta **43**, 19 (1991)
63. U.I. Safronova, W.R. Johnson, H.G. Berry, Phys. Rev. A **61**, 052503 (2000)
64. U.I. Safronova, Mol. Phys. **98**, 1213 (2000)
65. K.-N. Huang, At. Data Nucl. Data Tab. **34**, 1 (1986)
66. D.R. Beck, P.L. Norquist, Phys. Rev. A **61**, 044504 (2000)
67. U.I. Safronova, M. Sataka, W.R. Johnson, M.S. Safronova, JAERI-Data/Code 2001-022
68. C. Jupén, L.J. Curtis, Phys. Scripta **53**, 312 (1996)
69. C. Jupén, B. Denne, I. Martinson, Phys. Scripta **41**, 669 (1990)
70. K.-N. Huang, At. Data Nucl. Data Tab. **32**, 503 (1985)
71. Y. Ishikawa, M.J. Vilkas, Phys. Scripta **65**, 219 (2002)
72. M.J. Vilkas, Y. Ishikawa, J. Phys. B: At. Mol. Opt. Phys. **37**, 1803 (2004)
73. E. Träbert, A.G. Calamai, G. Gwinner, E.J. Knystautas, E.H. Pinnington, A. Wolf, J. Phys. B: At. Mol. Opt. Phys. **36**, 1129 (2003)
74. C. Jupén, I. Martinson, B. Denne-Hinnov, Phys. Scripta **44**, 562 (1991)
75. P. Bengtsson, K. Ando, T. Kambara, Y. Awaya, R. Hutton, Phys. Scripta T **73**, 81 (1997)
76. E. Träbert, Phys. Scripta **59**, 443 (1999)
77. M. Huang, R. Hutton, Y. Zou, K. Ando, H. Oyama, Nucl. Instrum. Meth. Phys. Res. B **205**, 119 (2003)
78. M. Huang, M. Andersson, T. Brage, R. Hutton, P. Jönsson, C. Chonyang, Y. Zou, J. Phys. B: At. Mol. Opt. Phys. **38**, 503 (2005)
79. K.-N. Huang, At. Data Nucl. Data Tab. **30**, 313 (1984)
80. E. Träbert, S. Fritzsche, C. Jupén, Eur. Phys. J. D **3**, 13 (1998)
81. A.W. Weiss, Y.-K. Kim, Phys. Rev. A **51**, 4487 (1995)
82. A.E. Livingston, R. Büttner, A.S. Zacarias, B. Kraus, K.-H. Schartner, F. Folkmann, P.H. Mokler, J. Opt. Soc. Am. **14**, 522 (1997)
83. E. Träbert, P. Beiersdorfer, E.H. Pinnington, S.B. Utter, M.J. Vilkas, Y. Ishikawa, *Proc. Conf. on the Physics of Highly Charged Ions* (HCI-2006), J. Phys. Conf. Ser. (to be published)
84. R. Hutton, Phys. Scripta T **73**, 25 (1997)
85. Y. Zou, R. Hutton, S. Huldt, I. Martinson, K. Ando, T. Kambara, H. Oyama, Y. Awaya, Phys. Rev. A **60**, 982 (1999)
86. K.-N. Huang, W.R. Johnson, Nucl. Instrum. Meth. B **502**, 104 (1985)
87. E. Träbert, Phys. Scripta **48**, 699 (1993)
88. H.S. Kwong, P.L. Smith, W.H. Parkinson **25**, 2629 (1982)
89. B.C. Johnson, P.L. Smith, W.H. Parkinson, Astrophys. J. **308**, 1013 (1986)
90. E. Träbert, A. Wolf, J. Linkemann, X. Tordoir, J. Phys. B: At. Mol. Opt. Phys. **32**, 537 (1999)
91. H.S. Kwong, B.C. Johnson, P.L. Smith, W.H. Parkinson, Phys. Rev. A **27**, 3040 (1983)
92. E. Träbert, P.H. Heckmann, R. Hutton, I. Martinson, J. Opt. Soc. Am. B **5**, 2173 (1988)
93. E. Träbert, J. Suleiman, S. Cheng, H.G. Berry, R.W. Dunford, E.W. Kanter, C. Kurtz, A.E. Livingston, K.W. Kukla, F.G. Serpa, L.J. Curtis, Phys. Rev. A **47**, 3805 (1993)
94. R. Hutton, Phys. Scripta T **73**, 25 (1997)
95. V. Kaufman, E. Träbert, P.H. Heckmann, G. Möller, V. Lodwig, J.H. Blanke, Phys. Scripta **42**, 705 (1990)